

Dissertations and Theses

---

8-2016

## Tsunami Warning System

Amay Vijay Desai

Follow this and additional works at: <https://commons.erau.edu/edt>



Part of the [Oceanography and Atmospheric Sciences and Meteorology Commons](#)

---

### Scholarly Commons Citation

Desai, Amay Vijay, "Tsunami Warning System" (2016). *Dissertations and Theses*. 298.  
<https://commons.erau.edu/edt/298>

This Thesis - Open Access is brought to you for free and open access by Scholarly Commons. It has been accepted for inclusion in Dissertations and Theses by an authorized administrator of Scholarly Commons. For more information, please contact [commons@erau.edu](mailto:commons@erau.edu).

# **Tsunami Warning System**

A Thesis

Submitted to the Faculty  
of Embry-Riddle Aeronautical University

by

Amay Vijay Desai

In Partial Fulfillment of the

Requirements for the Degree

of

Master of Science in Electrical and Computer Engineering

August 2016

Embry-Riddle Aeronautical University

Daytona Beach, Florida

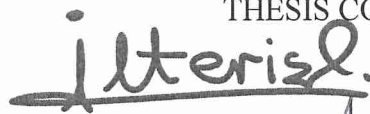
TSUNAMI WARNING SYSTEM

by

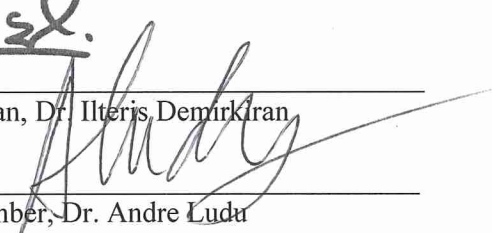
Amay Vijay Desai


A Thesis prepared under the direction of the candidate's committee chairman, Dr. Ilteris Demirkiran, Department of Electrical, Computer, Software & Systems Engineering, and has been approved by the members of the thesis committee. It was submitted to the School of Graduate Studies and Research and was accepted in partial fulfillment of the requirements for the degree of Master of Science in Electrical and Computer Engineering.


THESIS COMMITTEE

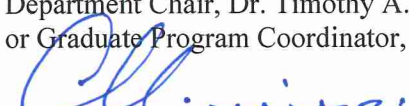


Chairman, Dr. Ilteris Demirkiran

  
Member, Dr. Andre Luda

  
Member, Dr. Tianyu Yang

  
Department Chair, Dr. Timothy A. Wilson  
or Graduate Program Coordinator, Dr. Jianhua Liu

  
Dean of College of Engineering, Dr. Maj Mirmirani

  
Vice Chancellor for Academics, Dr. Christopher D. Grant

26 Aug 2016  
Date

8/26/16  
Date

8/26/16  
Date

## **Acknowledgments**

First I would like to thank my thesis advisers Dr. Ilteris Demirkiran, Dr. Andre Ludu, and Dr. Tianyu Yang at Embry Riddle Aeronautical University. They have all always been available to help me solve all queries in my research and writing work. They steered me in the right direction to ensure successful completion.

Finally, I would like to express gratitude to my family for providing for giving me immense support and continuous encouragement throughout my studies. This accomplishment would not have been possible without them. Thank you.

## ABSTRACT

The effects of a tsunami on a coastline can be devastating. In an attempt to mitigate the damages caused by tsunamis, and to provide coastal communities with evacuation alerts, it is essential to have early warning systems installed offshore. Tsunami early warning systems can detect the formation of tsunami waves long before they reach shore, providing coastal communities with information about the strength of an incoming tsunami.

Since providing accurate information about oceanic wave patterns is absolutely necessary to forecast the magnitude of a tsunami as it forms, the focus of this research is to develop a novel approach which will predict the height and velocity of a tsunami long before it makes landfall. The research comprises of a mathematical study of how the objects under water appear would appear to any observer outside. Also included in the research is study of water surface regeneration techniques. The investigators believe that the proposed approach will provide unprecedented detail and accuracy to help forecast the magnitude of forming tsunami waves. This research will lay the groundwork for the next tsunami early warning system, which will continue to save lives in coastal communities around the world.

## Table of Contents

Chapter 1: Introduction .....	1
1.1 Background .....	1
1.2 Goals and Objectives.....	2
1.3 Thesis Outline .....	4
Chapter 2: Literature Review .....	5
2.1 History of Water Wave Research.....	5
2.2 Various approaches to Surface Wave and Image Reconstruction.....	8
Chapter 3: Mathematical approach to estimate object position .....	10
3.1 Object viewed in still water.....	10
3.1.1 Calculate the x component of X' .....	12
3.1.2 Calculate the y component of X' .....	14
3.1.3 Image formed on the lens.....	15
3.2 Water surface at an angle with the normal.....	16
3.2.1 Calculate the y component of X' .....	16
Chapter 4: Graphical Representation of derived equations .....	20
4.1 Case 1: [Water height h = 50 cm, Camera at 300 cm] .....	20
4.2 Case 2: [Water height h = 100 cm, Camera at 300 cm] .....	22
4.3 Case 3: [Water height h = 150 cm, Camera at 300 cm] .....	24
4.4 Case 4: [Water height h = 250 cm, Camera at 300 cm] .....	26
4.5 Case 5: [Object Distance = 50 cm, Camera at 300 cm] .....	28
Chapter 5: Summary and conclusion .....	30
Conclusion .....	44
Future Work .....	47
References.....	48
Appendix A Snell's Law.....	A
Appendix B Matlab Codes.....	C
Appendix C Mathematica Simulation And Theory .....	F

## Table of Figures

Figure 1: Camera Setup over Water Tank .....	2
Figure 2: Side view of camera setup.....	3
Figure 3: Object view by the camera .....	10
Figure 4: To calculate X component.....	12
Figure 5: Water Surface at an angle with the normal. ....	13
Figure 6: Plot of angle $\alpha'$ v/s Change in object position [Case 1].....	20
Figure 7: Plot of angle $\beta'$ v/s Change in object position. [Case 1].....	21
Figure 8: Plot of Virtual Height of X' v/s Change in object position [Case 1] .....	21
Figure 9: Plot of angle $\alpha'$ v/s Change in object position [Case 2].....	22
Figure 10: Plot of angle $\beta'$ v/s Change in object position. [Case 2].....	23
Figure 11: Plot of Virtual Height of X' v/s Change in object position [Case 2] .....	23
Figure 12: Plot of angle $\alpha'$ v/s Change in object position [Case 3].....	24
Figure 13: Plot of angle $\beta'$ v/s Change in object position. [Case 3].....	25
Figure 14: Plot of Virtual Height of X' v/s Change in object position [Case 3] .....	25
Figure 15: Plot of angle $\alpha'$ v/s Change in object position [Case 4].....	26
Figure 16: Plot of angle $\beta'$ v/s Change in object position. [Case 4].....	27
Figure 17: Plot of Virtual Height of X' v/s Change in object position [Case 4] .....	27
Figure 18: Plot of angle $\alpha'$ v/s Change in water height. ....	28
Figure 19: Plot of angle $\beta'$ v/s Change in water height .....	29
Figure 20: Plot of Virtual Height of X' v/s Change in Water height.....	29
Figure 21: : Diagram of vectors for the full 3-dimensional calculations.....	30
Figure 22: Sine wave Generator .....	38
Figure 23: Grid placement inside the tank.....	38
Figure 24: Waves captured using high speed camera.....	39
Figure 25: Overhead view of the waves moving over the grid.....	39
Figure 26: Height measured using oscilloscope .....	40
Figure 27: Comparison of heights using numerical method rapid camera and level gauges. ....	40
Figure 28: Irregular waves compared using the three listed methods .....	41
Figure 29: Y component Vs Water height .....	43

Figure 30: The Predicted result Using Mathematica .....	44
Figure 31: Image of a coin with no water .....	46
Figure 32: Image of a coin with 1 inch water .....	46



## **Chapter 1: Introduction**

In this chapter, the overview of the thesis research will be covered. It includes some background on wave study, purpose of the thesis and its organization.

### **1.1 Background**

Nature and its forces will continue impacting and affecting all living and non-living aspects of the earth. Some of these godly phenomenon are water-waves, wind-waves and the interactions between the air and the sea. The study of this subject has its applications not only in science but in engineering as well. The off-shore and floating platforms require structural engineers to study the stability and impact of the wave forces on the platform. Enhancing current ship designs requires naval engineers to have knowledge of water waves. Marine biologists are interested in learning how gas and mineral transfer takes place between the two surfaces and its effect on marine life. Hence the study of free-surface flows, which are complex and not yet fully understood rouse a lot of interest among people of varied backgrounds.

The investigators study of water waves begins with the initial assumption that the change in height of water leads to changes in the magnification and apparent distortion of objects under water. The study tries to correlate magnification and water height thus helping the investigators predict the water height while comparing magnification to two consecutive images. This research could help judge the size of any waves which will be the stepping stone towards the tsunami warning system.

## 1.2 Goals and Objectives

The goal of this thesis is to provide an effective way to study about various aspects of water-waves and also a mathematical approach to how objects in shallow water would appear to any observer on the outside. In the proposed study, a digital imaging camera will be located above the water so that its optical axis will be perpendicular to the water's surface. The grid, or frame of interest, is located at the bottom of the water tank.

The figures below illustrate an example where the camera observes the grid through the water surface.

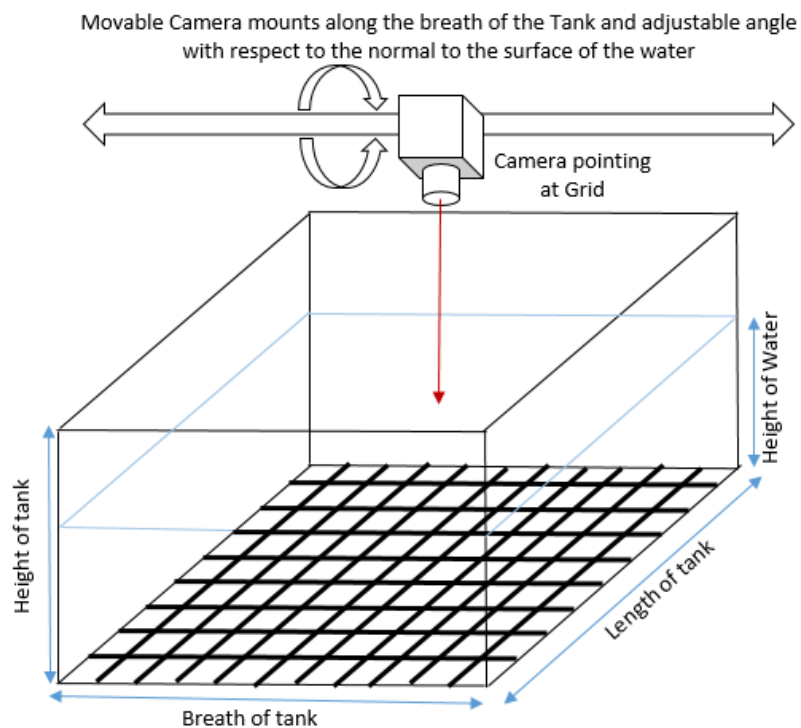


Figure 1: Camera Setup over Water Tank.

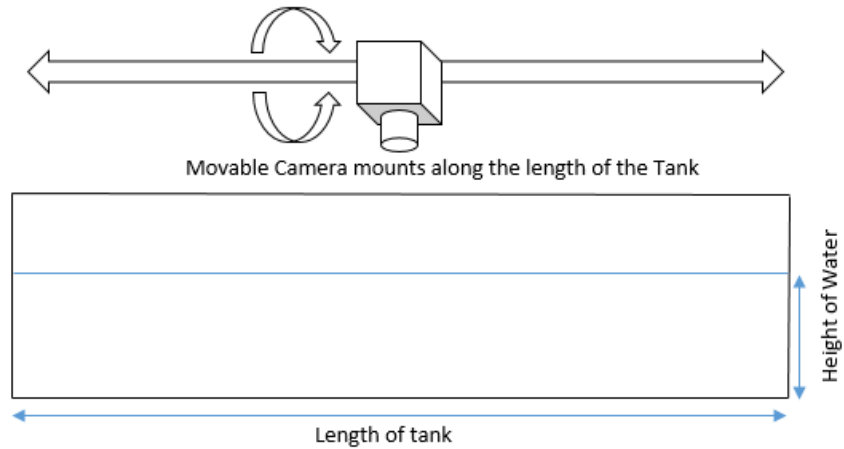


Figure 2: Side view of camera setup

This thesis also compares methods to reconstruct the surface of the water.

To meet the goal, following objectives were enumerated.

1. Design a program to perform data analysis, statistics and modeling.
2. Build experimental setup, probably stereo photography, backed up by rapid camera videos and by height gauges for height.
3. Identify the magnitude of the water wave by analyzing the pictures of the objects in the absence and the presence of water fluctuations.
4. Derive unique Mathematical equations which define how the objects under water are viewed by an overhead camera.
5. Compare and test various surface regeneration techniques and improve on existing algorithms.

### **1.3 Thesis Outline**

In the following chapters of the report, the proposed study is detailed.

Chapter 2 includes literature review to discuss initial study and different aspects of water wave theory.

Chapter 3 has detailed derivations of the researcher's mathematical approach towards how an object under water is viewed through a camera lens versus how the object actually appears.

Chapter 4 is a graphical representation of the mathematical equations derived and its comparison to previous assumptions.

Chapter 5 covers the conclusions and results.

## Chapter 2: Literature Review

This chapter will focus on all the literature needed for the Research. It will discuss the initial study of water waves and varied approaches to surface reconstruction algorithms.

### 2.1 History of Water Wave Research.

To begin the study on water waves, the researchers will review on the origins of this theory before the 20th century which was done extensively in Craik (2004). Sir Isaac Newton (1687) first attempted to devise a theory of water-waves, whose work was followed by Gravesande (1721) and Charles Bossut (1786), while the equations of hydrodynamics were derived by Euler (1757a, 1757b, 1761).

Wave motion was reexamined by Laplace and posed the general initial value problem in Laplace (1799). Lagrange (1781, 1786) derived linearized governing equations for small-amplitude waves and obtained the solution in the limiting case of long plane waves in shallow water.

The first exact nonlinear solution for waves of finite amplitude in deep water was given by Gerstner (1802). Young (1821) wrote extensively on tides, but briefly on waves. In 1818 and 1827 Cauchy-Poisson analysis was presented, and although Dalmedico (1988) highlighted errors in the fundamental equations, it is one of the most important contributions in the mathematical theory of initial-value problems.

Vince (1798), a British scientist, published on Hydrodynamics. Pratt (1836) had brief section on the equations of inviscid flow. Green, Kelland, airy and Earnshaw published on water waves during the following years. Kelland's (1844) analysis considered the wave-motion in a fluid of finite depth, on the hypothesis of parallel sections considering long waves in shallow water, what is now called the Stokes

frequency correction. Kelland's study of waves in canals with non-rectangular cross sections is also noteworthy. Earnshaw (1847) began with an intro for solitary waves and arrived at the results for horizontal velocity and water depth for the wave speed. Eventually, Rayleigh derived the correct approximate solution, retaining both dispersion and nonlinearity and further observed that Earnshaw's solution is not irrotational.

Although Airy's (1841, 1845) main focus of interest was tidal phenomena, he also wrote a substantial section on the Theory of Waves in Canals in 1841 and an Account of Experiments on Waves in 1845. Much of the work is original and concerned with modelling observed or observable phenomena. Airy gave the now-standard linear theory for plane waves and his theory gives very good approximate prediction of water waves but it is not applicable to predict steep waves and non-linear waves observed in the oceans.

The first person to put forward almost all the previous work in one place including his work describing linear mathematical models governing water waves and the analytical theory for wind-waves was Sir Horace Lamb (1930). The possibility that separation of the airflow might occur at each wave crest and produce a region of low velocity and low pressure downwind of the crest was pointed out by Jeffreys (1924b, 1924a, 1925). Thus there would be a difference in pressure between upwind and downwind faces of the wave able to transfer energy from the wind to the wind-waves. However, the generally observed rate of growth of wind-waves is lower than Jeffreys (1924b) calculation.

Seminal work on shear flow theory on the generation of surface waves by wind was presented by John Miles (1957) with certain assumptions in shear flow theory such as air flow is assumed to be inviscid, incompressible and has some specified mean shear flow in the absence of waves. The disturbances in the air flow induced by the surface waves are assumed to be two dimensional and small enough so that the equations of motion are linearized. The turbulent fluctuations which must be present to maintain the mean shear flow are neglected in the perturbation equations. The assumption is that the water is inviscid, incompressible, irrotational and has small surface slopes along with no mean drift currents. Furthermore, the wave speed is assumed to be unaltered by any push by the wind and the wind speed is considered low compared to the wave speed.

All the above assumptions leads to inappropriate energy extraction and subsequently underestimate the wave growth due to wind-wave interaction. The theory is found to under-predict the wave growth rate by a factor of 8 to 10 on comparing with fieldwork studies by Snyder & Cox (1966), Barnett & Wilkerson (1967) and laboratory studies by Bole & Hsu (1969). The resonance model of Phillips (1957) includes direct action of turbulent pressure fluctuations on the water surface but neglects any interactions between wave field and pressure field. It is an uncoupled model in the sense that the response is assumed to be independent from excitation and the wind profile over the waves is assumed to be logarithmic.

Moreover, the theory by Phillips (1957) relies on turbulent pressure fluctuations to provide a random force acting onto the wave surface, ensuring wind-to-wave energy transfer and leading to a linear increase in wave amplitude in time. However, most of the researchers have found this assumption invalid in real ocean measurements. This

proves that distribution of stress on the surface is a function of the pressure field and also the coupled instability mechanism. Kinsman (1965) has done detailed analysis about the effect of resonant wave and shear flow and has written extensively about the combined model (resonance and shear flow) and the nonlinear wind-wave model for surface waves.

## **2.2 Various approaches to Surface Wave and Image Reconstruction.**

Surface reconstruction has now been a widely researched subject and its primary purpose is to study the wave structure. The researchers have presented a brief study of surface reconstruction with the idea of comparing images distorted by water waves to its reconstructed images thus giving an approximate idea of the water surface shape and features. Thus the below study would point out various researches conducted in image recovery, image reconstruction and surface reconstruction.

The main approach to surface reconstruction has been to extract the shape of water surfaces from images of water [10, 11, 12, 13]. This work done by those in the computer vision community as well as those in oceanography sought to take advantage of water's optical properties to reconstruct a surface. Techniques developed to utilize water's refractivity to reconstruct a surface have had much more success than those using the reflectivity property of water [9, 10].

Any transparent object moving above a certain surface causes distortion in the appearance of the lower surface due to refraction at its surface. Most refraction methods use a single viewpoint and assume an orthographic projection [13, 15, 16]. Murase (1992) [5, 13] describes an algorithm to reconstruct the surface shape of the non-rigid transparent object from the apparent motion of the observed pattern. He has



achieved this by extracting the optical flow sequence of consecutive images of the distorted surface, averaging their trajectory thus calculating the surface normal and reconstructing the surface. This method shares certain similarities with another method called shape from motion. Two major difference between these two methods is

(1) The latter involves 3-D structure reconstruction using movements of several points on the object based on an assumption of rigidity [6].

(2) Murase's algorithm uses points on the refracted images rather than points on the object.

The drawbacks of Murase's algorithm was the accuracy of the extraction of optical flow impacted the final result. Also, his method requires a relatively distant camera to minimize projection distortion.

Morris [14] avoids certain assumptions and inaccuracies of previous methods by using stereo cameras to capture images of a pattern refracted through water. His research builds on work that utilizes refractive distortion as well as stereo reconstruction research. His system was based upon finding individual points on the water surface.

## Chapter 3: Mathematical approach to estimate object position

In this section, the investigators derive the measurement technique in detail and compare it to theoretical results.

### 3.1 Object viewed in still water

The investigators have set up the experiment as shown in the figure below.

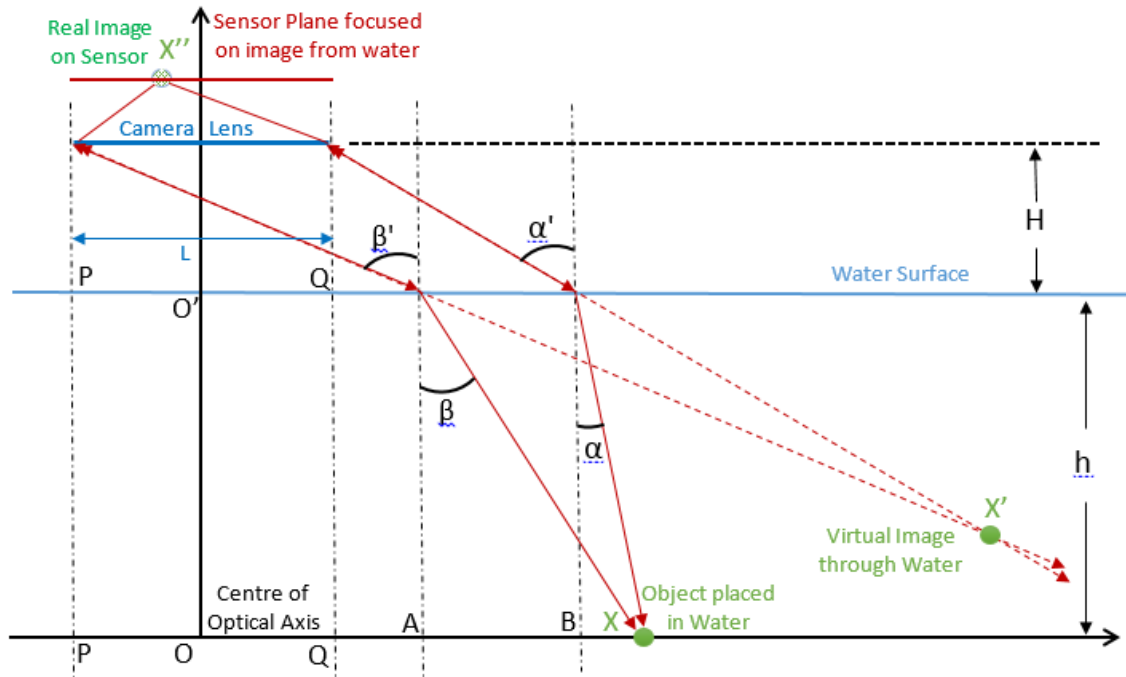


Figure 3: Object view by the camera

As seen in figure 3, the camera of lens Diameter ' $L$ ' is placed such that the centre of the optical axis is perpendicular to the surface of water and ground. The object is considered to be a point source " $X$ " on the surface whose distance will be varied along the  $X$  axis for experimental simplicity.

As shown in the figure the light travelling from the point source to the two extremities of the camera while creating angles " $\alpha$ " and " $\beta$ " at the surface of the water.

Thus, due to Snell's law (Appendix A), the angles “ $\alpha$ ” and “ $\beta$ ” will get diffracted and form “ $\alpha'$ ” and “ $\beta'$ ” as the rays of light reach the camera. Due to refraction across water, the virtual image is seen at point “X”.

Given Distance of object 'X' from the Centre of optical axis 'O', we calculate the angles by which light gets refracted as it reaches the lens

From figure 1, we calculate the two angles ' $\alpha$ ' and ' $\beta$ ' with respect to the 'x':

$$x = XB + BA + AQ + QO \quad \text{eq. (1)}$$

'x' in terms of angle ' $\alpha$ '

Using trigonometric properties eq. (1) can be re-written as:

$$x = h * \tan(\alpha) + H * \tan(\alpha') + \frac{L}{2} \quad \text{eq. (2)}$$

Snell's Law,  $n_1 \sin \theta_1 = n_2 \sin \theta_2$ , is used to calculate.... (Appendix A)

Using Snell's Law, the visual displacement of the object in water was calculated in this manner:

$$n * \sin(\alpha) = \sin(\alpha') \quad \text{eq. (3)}$$

$$x = h * \tan(\alpha) + H * \frac{\sin(\alpha')}{\cos(\alpha')} + \frac{L}{2} \quad \text{eq. (4)}$$

Substituting eq. (3) in eq. (4)

$$x = h * \tan(\alpha) + H * \frac{\sin(\alpha)}{\sqrt{1-n^2 \sin^2(\alpha)}} + \frac{L}{2} \quad \text{eq. (5)}$$

Similarly for 'x' in terms of angle ' $\beta$ '

$$x = h * \tan(\beta) + H * \frac{\sin \beta}{\sqrt{1-n^2 \sin^2(\beta)}} - \frac{L}{2} \quad \text{eq. (6)}$$

### 3.1.1 Calculate the x component of X'

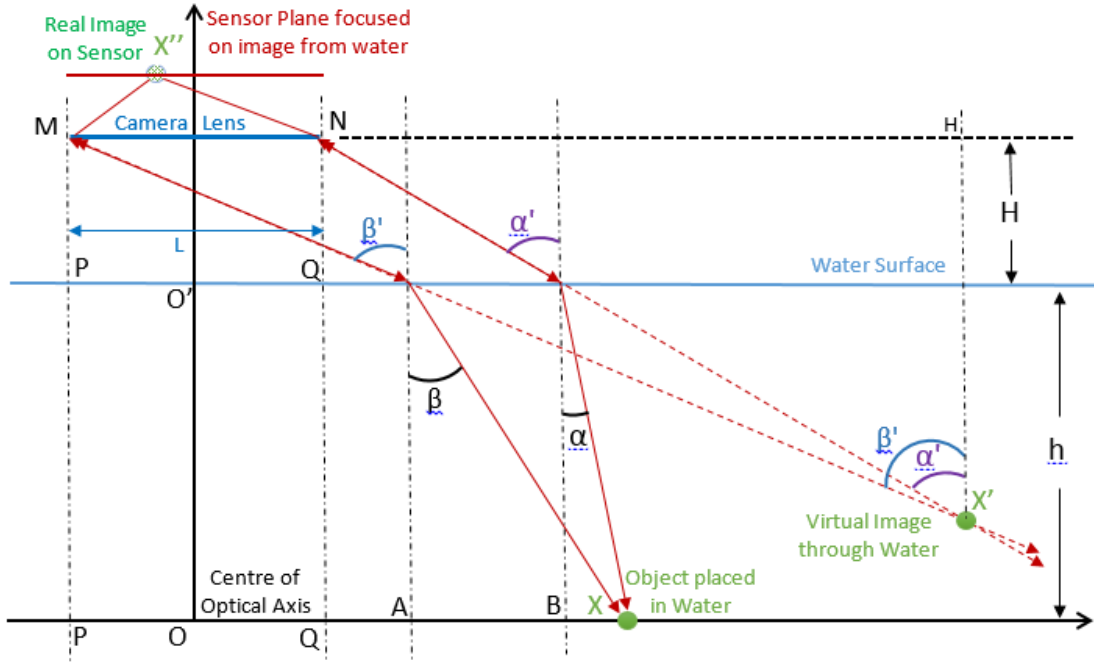


Figure 4: To calculate X Component

Consider angle  $\alpha'$  at the vertex  $X'$  of triangle  $NX'H$ ,

$$\tan(\alpha') = \frac{NH}{HX'} \quad \text{eq. (7)}$$

Which can be re written as:

$$HX' = \frac{NH}{\tan(\alpha')} \quad \text{eq. (8)}$$

Similarly, considering angle  $\beta'$  at vertex  $X'$  of the triangle  $MX'H$ ,

$$\tan(\beta') = \frac{MH}{HX'} \quad \text{eq. (9)}$$

But  $MH = MN + NH$  As seen in figure 2,

$$\text{Hence, } \tan(\beta') = \frac{MN+NH}{HX'} \quad \text{eq. (10)}$$

But  $MN = L$ ,

Thus eq. 10 can be re written as

$$\tan(\beta') = \frac{L+NH}{HX'} \quad \text{eq. (11)}$$

Now substituting the value of  $HX'$  from Eq. (8) in eq. (11),

We get,

$$\tan(\beta') = \frac{L+NH}{\frac{NH}{\tan(\alpha')}} \quad \text{eq. (11)}$$

i.e.

$$\tan(\beta') = \frac{L+NH}{NH} * \tan(\alpha') \quad \text{eq. (12)}$$

Simplifying and equating in terms of  $NH$ , we have:

$$NH = \frac{L*\tan(\alpha')}{\tan(\beta') - \tan(\alpha')} \quad \text{eq. (13)}$$

From figure we can see that X component of  $X'$  is  $NH + \frac{L}{2}$

Therefore,

$$X \text{ component of } X' = \frac{L*\tan(\alpha')}{\tan(\beta') - \tan(\alpha')} + \frac{L}{2} \quad \text{eq. (14)}$$

### 3.1.2 Calculate the y component of X'

Consider angle  $\alpha'$  at the vertex X' of triangle NX'H,

$$\tan(\alpha') = \frac{NH}{HX'} \quad \text{Same as eq. (7)}$$

From figure 2, it can be seen that  $HX = HC' + C'X'$  and  $HX = H$ .

$$\tan(\alpha') = \frac{NH}{H+C'X'} \quad \text{eq. (15)}$$

Similarly,

$$\tan(\beta') = \frac{L+NH}{HX'} \quad \text{Same as eq. (11)}$$

$$\tan(\beta') = \frac{L}{H+C'X'} + \frac{NH}{H+C'X'} \quad \text{eq. (16)}$$

Substituting  $\tan(\alpha')$  from eq. (7)

$$\tan(\beta') = \frac{L}{H + C'X'} + \tan(\alpha')$$

Simplifying and equating in terms of  $C'X'$ , we have:

$$C'X' = \frac{L}{\tan(\beta') - \tan(\alpha')} - H$$

But  $h - C'X' = Y$  component of  $X'$ ; hence the final result for the Y component will be:

$$Y \text{ component of } X' = h - \frac{L}{\tan(\beta') - \tan(\alpha')} + H \quad \text{eq. (17)}$$

### 3.1.3 Image formed on the lens

Using Thin Lens Formula:

$$\frac{1}{\text{Focal Length}} = \frac{1}{\text{Object Distance}} + \frac{1}{\text{Image Distance}}$$

From Figure 3 we see the following:

$$\frac{1}{f} = \frac{1}{X'H} + \frac{1}{CO''}$$

$$\frac{1}{f} = \frac{1}{H+h-Y \text{ component of } X'} + \frac{1}{CO''} \quad \text{eq. (18)}$$

### 3.2 Water surface at an angle with the normal

For the next case, the investigators consider the surface of the water to be inclined to the normal as seen in the figure below.

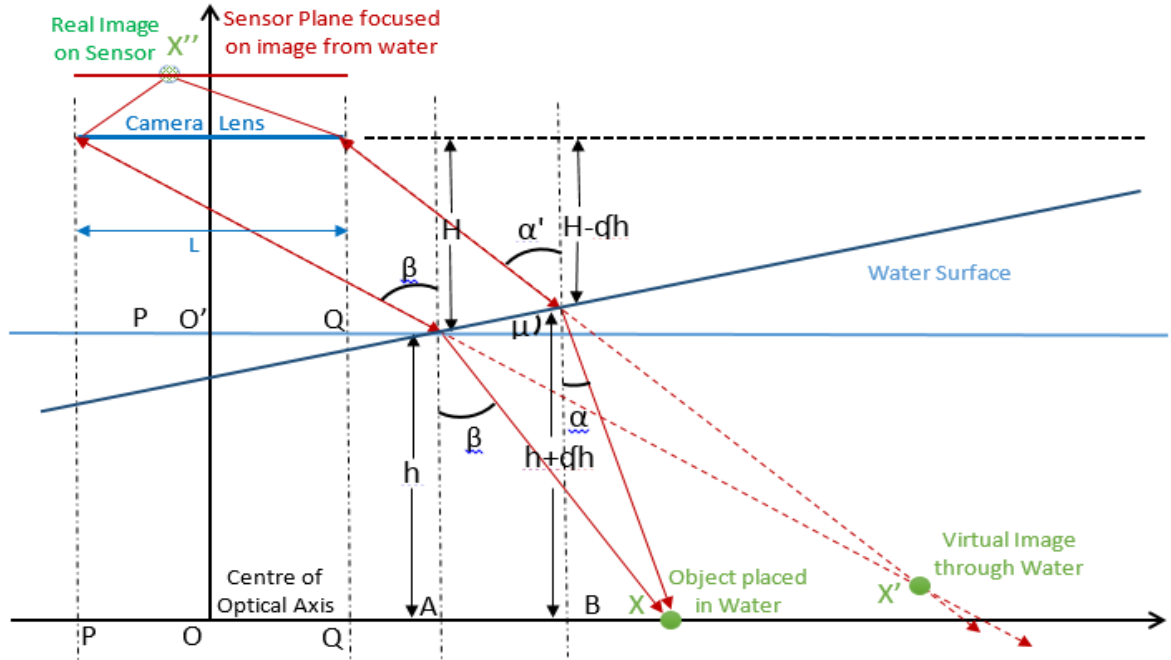


Figure 5: Water Surface at an angle with the normal.

#### 3.2.1 Calculate the y component of X'

Given Distance of object 'X' from the Centre of optical axis 'O', we calculate the angles by which light gets refracted as it reaches the lens

From figure 1, we calculate the two angles ' $\alpha$ ' and ' $\beta$ ' with respect to the 'x':

$$x = XB + BA + AQ + QO \quad \text{eq. (19)}$$

'x' in terms of angle ' $\beta$ '



$$x = h * \tan(\beta) + H * \frac{\sin \beta}{\sqrt{1-n^2 \sin^2(\beta)}} - \frac{L}{2} \quad \text{eq.(20)}$$

Hence 'x' in terms or angle 'α'

Using trigonometric properties eq. (1) can be re-written as:

$$x = (h + \text{d}h) * \tan(\alpha) + (H - \text{d}h) * \tan(\alpha') + \frac{L}{2} \quad \text{eq. (21)}$$

Using Snell's Law

$$n * \sin(\alpha) = \sin(\alpha') \quad \text{eq. (22)}$$

$$x = (h + \text{d}h) * \tan(\alpha) + (H - \text{d}h) * \frac{\sin(\alpha')}{\cos(\alpha')} + \frac{L}{2} \quad \text{eq. (23)}$$

Substituting eq. (4) in eq. (5)

$$x = (h + \text{d}h) * \tan(\alpha) + (H - \text{d}h) * \frac{\sin(\alpha)}{\sqrt{1-n^2 \sin^2(\alpha)}} + \frac{L}{2} \quad \text{eq. (24)}$$

We have:

$$AB = h * \tan(\beta) - (h + \text{d}h) * \tan(\alpha) \quad \text{eq. (25)}$$

and from:

$$\text{d}h = \tan(\mu) * AB$$

we obtain:

$$\text{d}h = \frac{h * (\tan(\beta) - \tan(\alpha))}{\cot(\mu) + \tan(\alpha)} \quad \text{eq. (26)}$$

We substitute the expression for d from eq. (26) in eq. (24) and obtain:

$$x = \left( h + \frac{h * (\tan(\beta) - \tan(\alpha))}{\cot(\mu) + \tan(\alpha)} \right) * \tan(\alpha) + \left( H - \frac{h * (\tan(\beta) - \tan(\alpha))}{\cot(\mu) + \tan(\alpha)} \right) * \frac{\sin(\alpha)}{\sqrt{1 - n^2 \sin^2(\alpha)}} + \frac{L}{2}$$

eq. (27)

In the following we consider the parameters H, h, L and n known, given and constant.

The next step is the solve eq. (20=2) for  $\beta$  and to obtain as solution the function  $\beta(x)$ , and then plug this  $\beta(x)$  expression in eq. (27):

$$x = \left( h + \frac{h * (\tan(\beta(x)) - \tan(\alpha))}{\cot(\mu) + \tan(\alpha)} \right) * \tan(\alpha) + \left( H - \frac{h * (\tan(\beta(x)) - \tan(\alpha))}{\cot(\mu) + \tan(\alpha)} \right) * \frac{\sin(\alpha)}{\sqrt{1 - n^2 \sin^2(\alpha)}} + \frac{L}{2}$$

eq. (28)

Then, solve eq. (28) with respect to  $\alpha$  and denote its solution by  $\alpha(x)$ .

At this point we have four given fixed input constant parameters H, h, L, n and 2 functions  $\alpha(x)$ ,  $\beta(x)$  probably in numeric solution (not analytic) form.

### Correct determination of h

The way h is used in these calculations is h="height of the free surface of water at point A"

Let us consider the free surface of water is described in general by the equation

$$y_{Free\ surface} = y_{\Sigma}(x, t) \quad \text{eq. (29)}$$

which in the present slated surface case is, for example,

$$y_{\Sigma}(x, t) = h_0 + x \tan \mu$$

where  $h_0$  is the height of water right under the center of the lenses, at origin  $x=0$ . It implies we have to use in all equations above, instead of the constant  $h$ , the solution  $h(x)$  of the equation:

$$h \rightarrow y_{\Sigma}(x_A, t) = h = h_0 + x_A \tan \mu = h_0 + OA \tan \mu$$

By solving the equation above we have

$$h \rightarrow h(x) = \frac{(h_0 + x \tan \mu) \tan \beta}{1 + \tan \mu \tan \beta}$$

This observation completely changes the expressions in eqs. (20, 28). Namely we have:

$$x = \frac{(h_0 + x \tan \mu) \tan \beta}{1 + \tan \mu \tan \beta} * \tan(\beta) + H * \frac{\sin \beta}{\sqrt{1 - n^2 \sin^2(\beta)}} - \frac{L}{2} \quad \text{eq.(30)}$$

and

$$x = \frac{(h_0 + x \tan \mu) \tan \beta(x)}{1 + \tan \mu \tan \beta(x)} \left( 1 + \frac{\tan(\beta(x)) - \tan(\alpha)}{\cot(\mu) + \tan(\alpha)} \right) * \tan(\alpha) + (H - \frac{(h_0 + x \tan \mu) \tan \beta(x) \tan(\beta(x)) - \tan(\alpha)}{1 + \tan \mu \tan \beta(x) \cot(\mu) + \tan(\alpha)}) * \frac{\sin(\alpha)}{\sqrt{1 - n^2 \sin^2(\alpha)}} + \frac{L}{2} \quad \text{eq. (31)}$$

## Chapter 4: Graphical Representation of derived equations

In this chapter, the investigators implement the derived functions graphically and compare its results to the initial findings for various cases.

### 4.1 Case 1: [Water height $h = 50$ cm, Camera at 300 cm]

The Investigators attempt to verify the credibility of the derived equations for multiple cases using MATLAB (Appendix B). Assumptions made for case 1 are listed below:

- The camera is fixed at a height of 300 cms.
- The water level is said to be 50 cms.
- The object distance from the optical center is varied until total internal reflection occurs.

Figure 6 and figure 7 below show the angles “ $\alpha'$ ” and “ $\beta'$ ”.

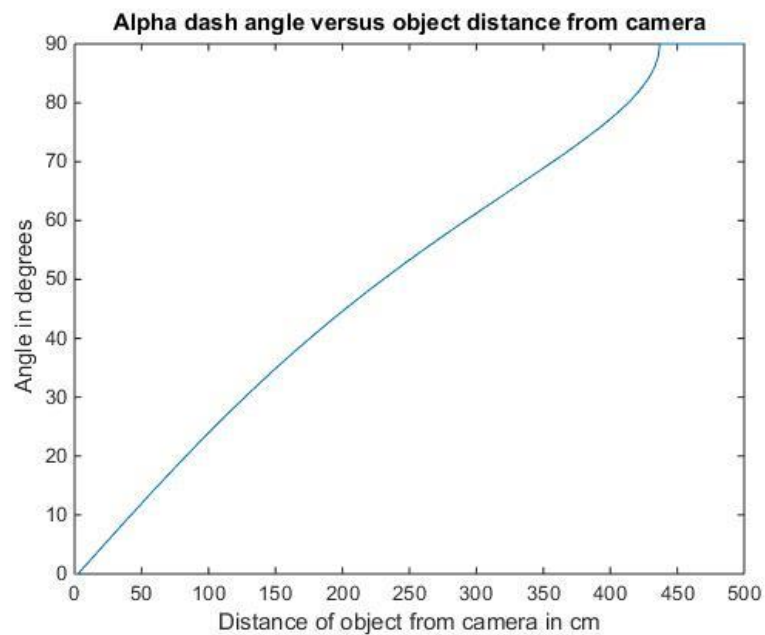


Figure 6: plot of angle  $\alpha'$  v/s Change in object position.

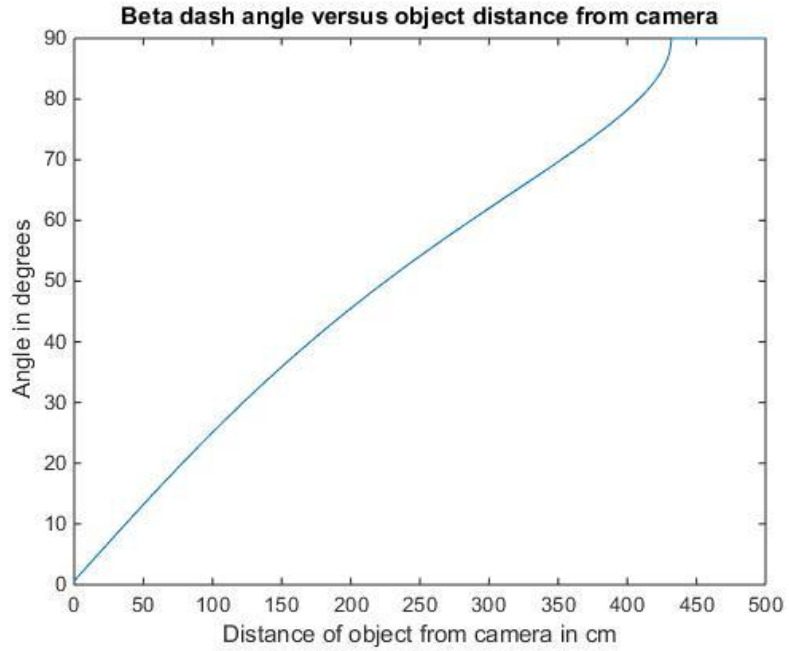


Figure 7: plot of angle  $\beta'$  v/s Change in object position.

Figure 8 displays the apparent height of the virtual image in water with change in object distance

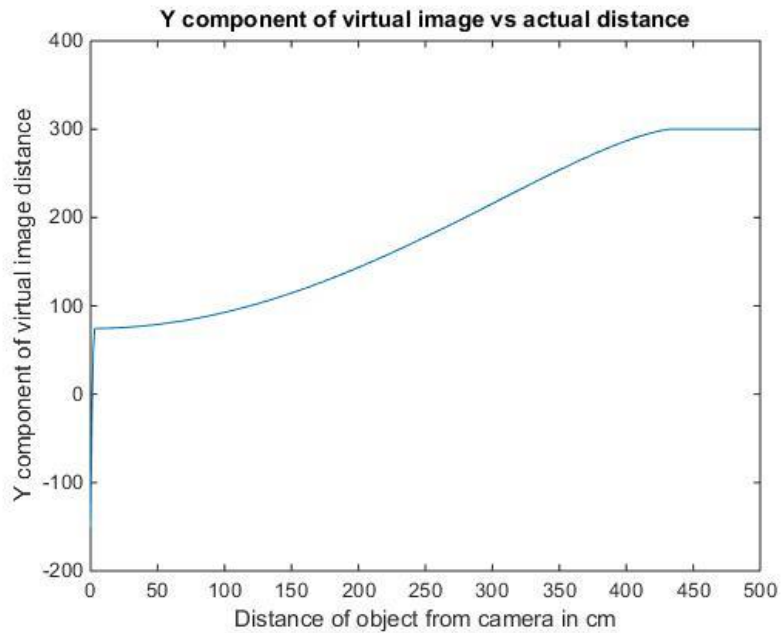


Figure 8: plot of Virtual Height of X' v/s Change in object position.

## 4.2 Case 2: [Water height $h = 100$ cm, Camera at 300 cm]

Assumptions made for case 2 are listed below:

- The camera is fixed at a height of 300 cms.
- The water level is said to be 100 cms.
- The object distance from the optical center is varied until total internal reflection occurs.

Figure 9 and figure 10 below show the angles “ $\alpha'$ ” and “ $\beta'$ ”.

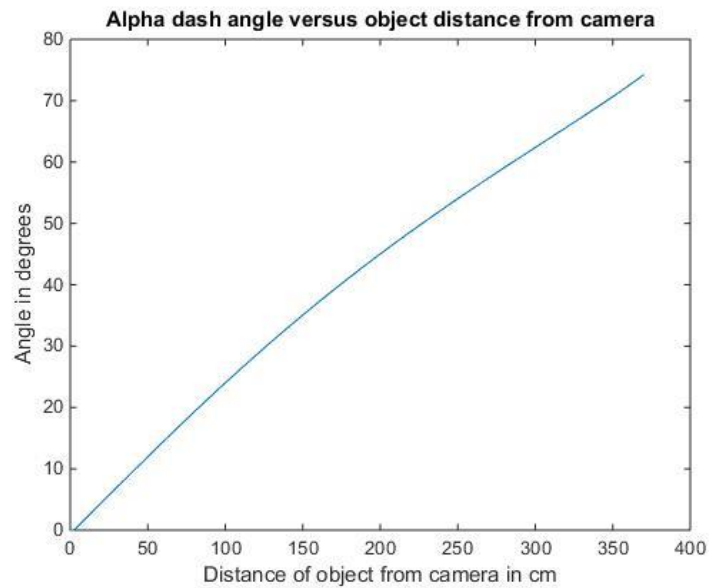


Figure 9: plot of angle  $\alpha'$  v/s Change in object position.

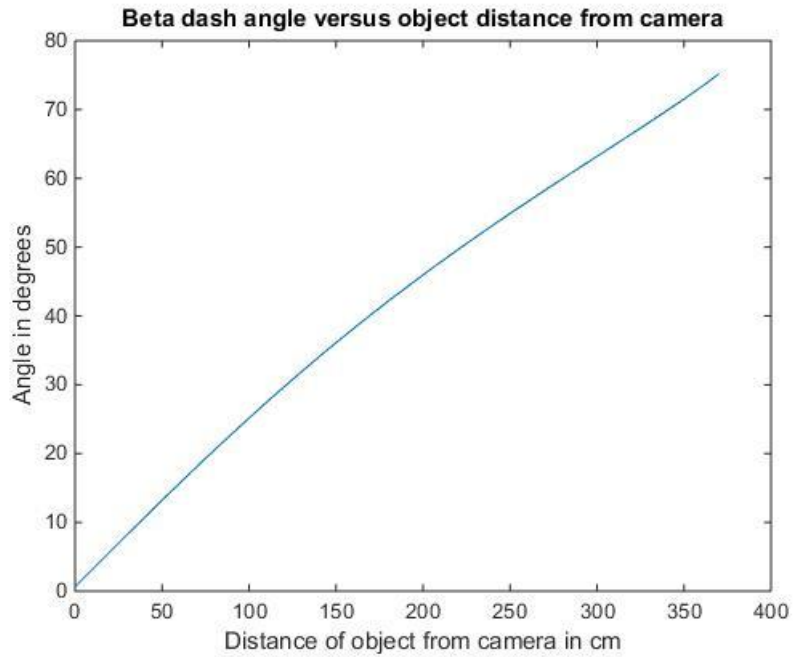


Figure 10: plot of angle  $\beta'$  v/s Change in object position.

Figure 11 displays the apparent height of the virtual image in water with change in object distance

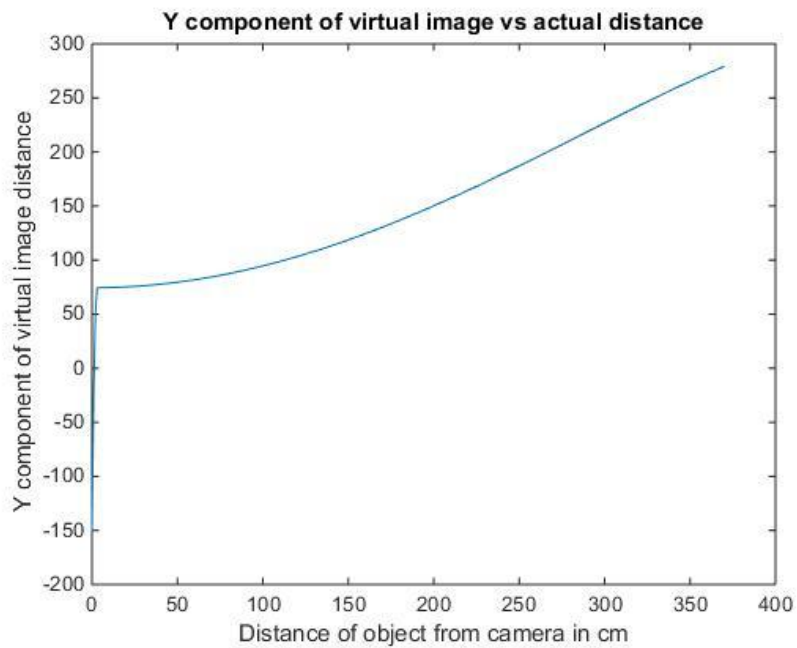


Figure 11: plot of Virtual Height of  $X'$  v/s Change in object position.

### 4.3 Case 3: [Water height $h = 150$ cm, Camera at 300 cm]

Assumptions made for case 3 are listed below:

- The camera is fixed at a height of 300 cms.
- The water level is said to be 150 cms.
- The object distance from the optical center is varied until total internal reflection occurs.

Figure 12 and figure 13 below show the angles “ $\alpha$ ’ ” and “ $\beta$ ’ ”.

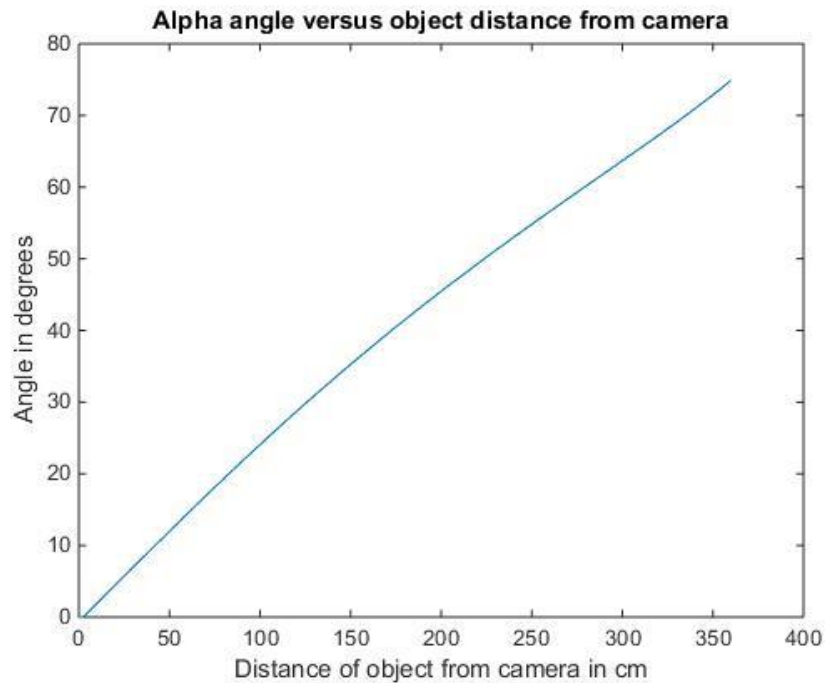


Figure 12: plot of angle  $\alpha$ ’ v/s Change in object position.



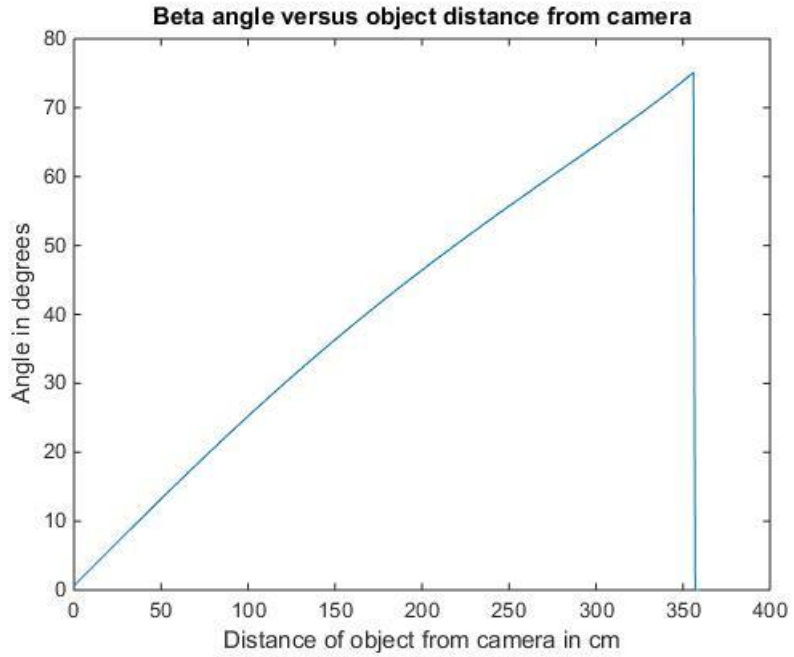


Figure 13: plot of angle  $\beta'$  v/s Change in object position.

Figure 14 displays the apparent height of the virtual image in water with change in object distance

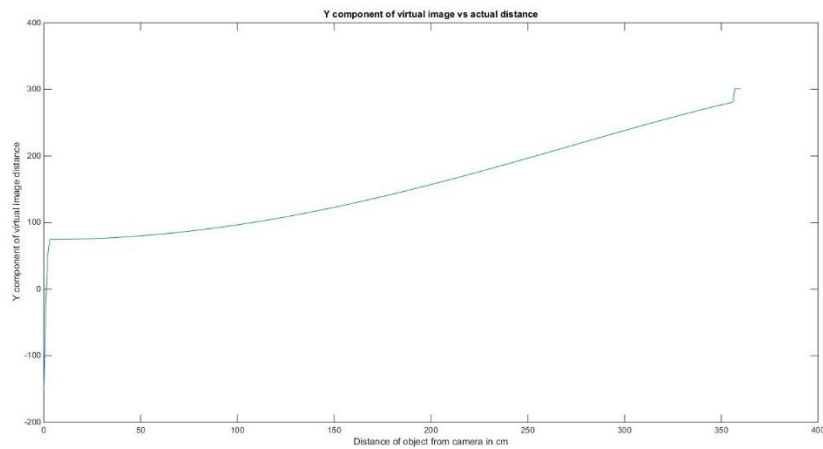


Figure 14: plot of Virtual Height of  $X'$  v/s Change in object position.

#### 4.4 Case 4: [Water height $h = 250$ cm, Camera at 300 cm]

Assumptions made for case 4 are listed below:

- The camera is fixed at a height of 300 cms.
- The water level is said to be 150 cms.
- The object distance from the optical center is varied until total internal reflection occurs.

Figure 15 and figure 16 below show the angles “ $\alpha$ ” and “ $\beta$ ”.

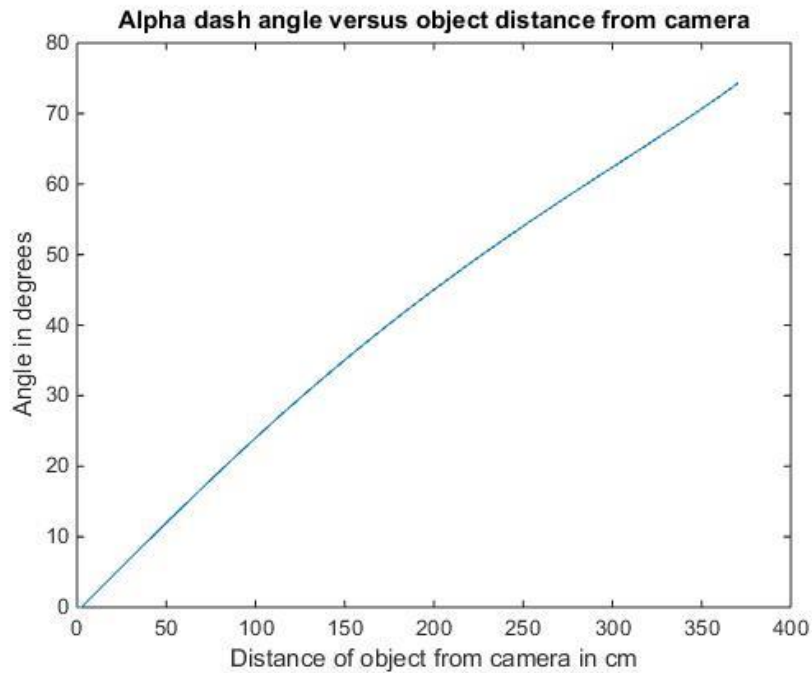


Figure 15: plot of angle  $\alpha'$  v/s Change in object position.

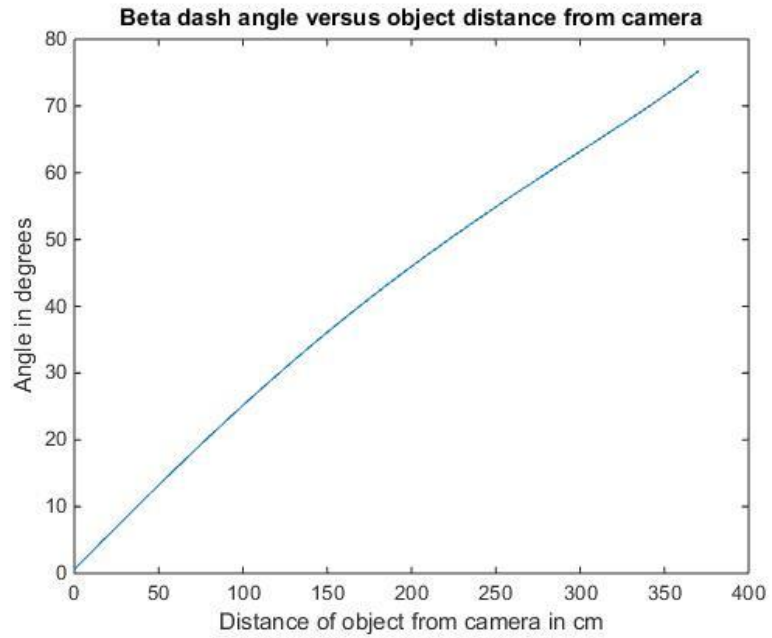


Figure 16: plot of angle  $\beta'$  v/s Change in object position.

Figure 17 displays the apparent height of the virtual image in water with change in object distance

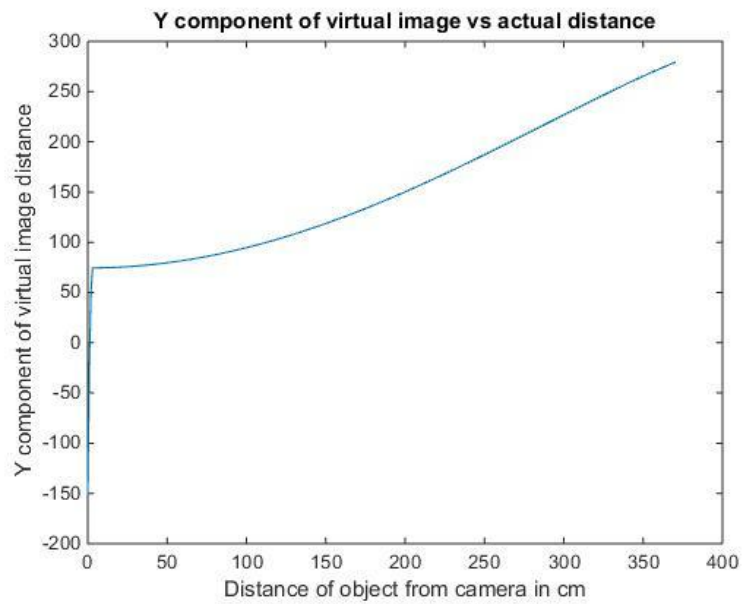


Figure 17: plot of Virtual Height of  $X'$  v/s Change in object position.

#### 4.5 Case 5: [Object Distance = 50 cm, Camera at 300 cm]

Assumptions made for case 5 are listed below:

- The camera is fixed at a height of 300 cms.
- The water level is changed from 0 to 200 cms.
- The object distance from the optical center is kept constant at 50 cm.

Figure 18 and figure 19 below show the angles “ $\alpha$ ” and “ $\beta$ ”.

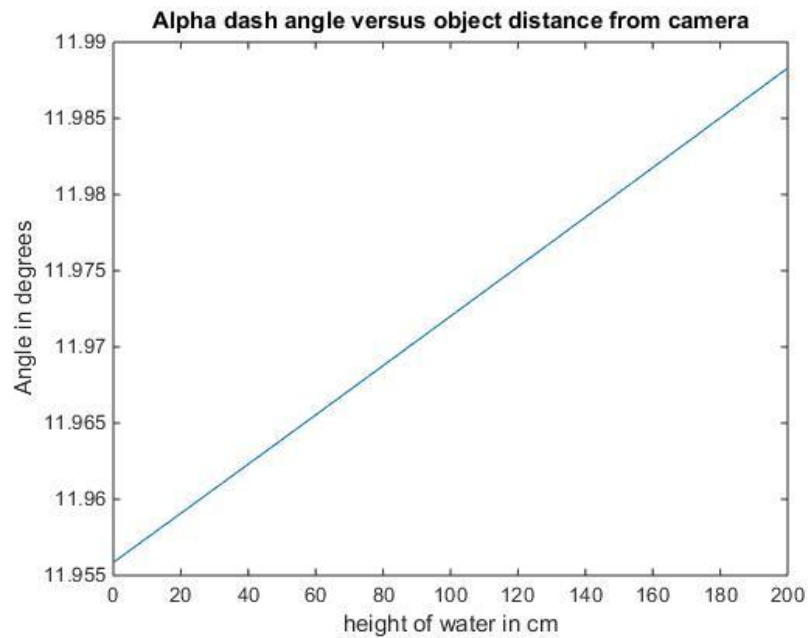


Figure 18: plot of angle  $\alpha'$  v/s Change in water height.

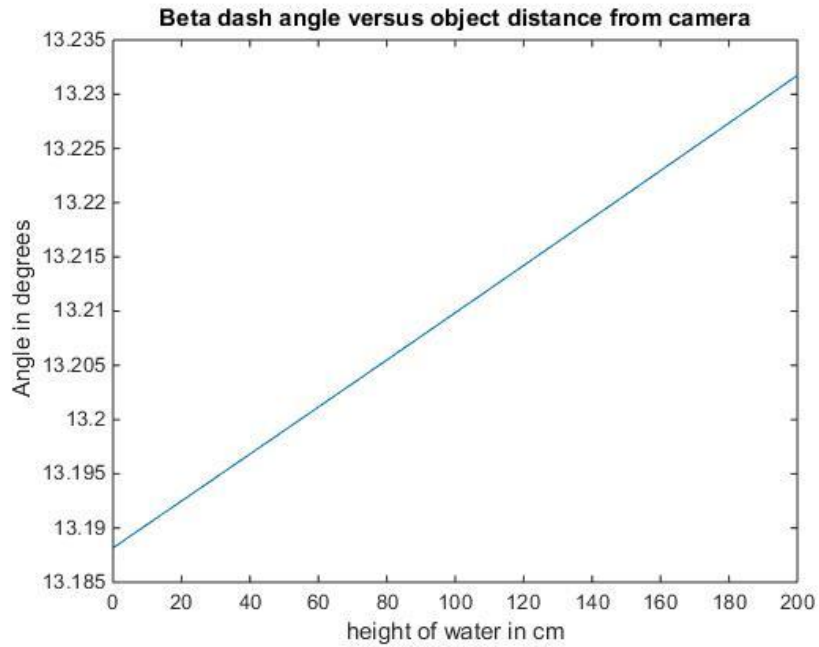
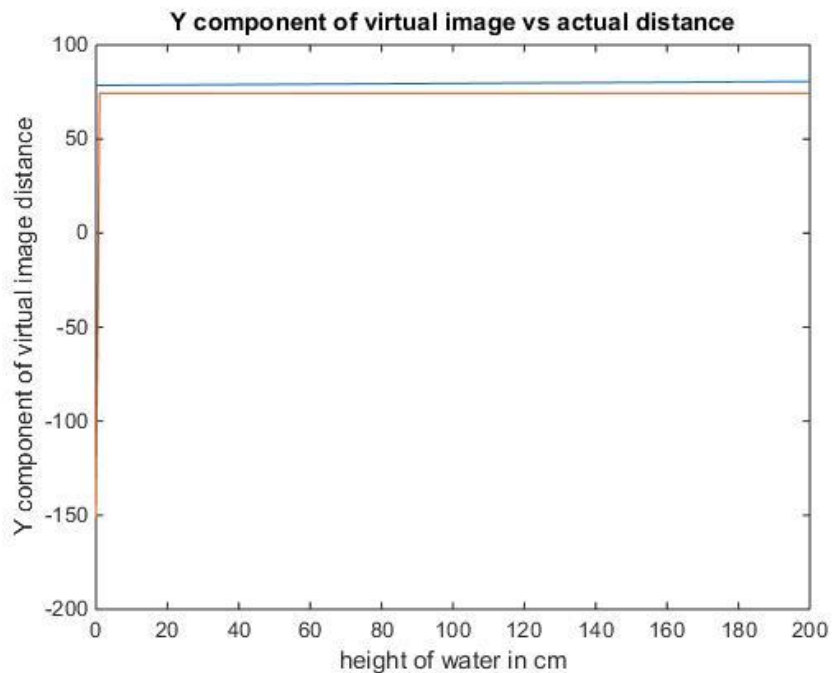


Figure 19: plot of angle  $\beta'$  v/s Change in water height.

Figure 20 displays the apparent height of the virtual image in water with change in water level

Figure 20: plot of Virtual Height of X' v/s Change in Water height.



## Chapter 5: Fully 3-dimensional calculations

In this chapter we present a full 3-dimensional calculation of the representation of the image through water surface of a flat bottom pattern into the camera sensors. All the vectors and geometrical quantities are presented grouped in Fig. 21 below. All the images and quantities are represent at a frozen moment of time  $t$ , so time does not occur explicitly in the equations below, yet anything can be made time dependent.

We consider the flat bottom of the water in the tank to be the horizontal plane ( $x$ ,  $y$ ), and  $z$  is the vertical upward axis. The front side of the lenses of the camera are represented by a horizontal disc of radius  $R$ , focal distance  $F$ , concentric with the  $z$  axis, and placed at a height  $H$  from the bottom,  $z_{\text{camera}}=H$ . The lenses are represented by the point  $L$  in Fig. 21, mainly because  $R \ll H$ . The water free surface is represented by the equation  $z = f(x, y)$ , namely a differentiable function. One possible working example is a standing sine wave of amplitude  $A$ , centered at equilibrium height  $h$ , and having wavelengths  $L_x, L_y$  along  $x$  and  $y$ , respectively:

$$f(x, y) = h + A \sin \frac{2\pi x}{L_x} \sin \frac{2\pi y}{L_y}.$$

Let us consider the object point  $X$  as one light point in the bottom pattern (for example the corner of a chess-board pattern) of coordinate  $(x, y, 0)$ . This point is represented by the horizontal vector  $\vec{X} = OX = (x, y, 0)$  and it makes the angle  $\varphi_X$  with  $x$ -axis. Let us send a ray of light out and upwards from point  $X$ , along the unit direction

$$\vec{e} = (\sin \theta \cos \varphi, \sin \theta \sin \varphi, \cos \theta), \quad \|\vec{e}\| = 1,$$

where  $0 \leq \theta \leq \frac{\pi}{2}, 0 \leq \varphi \leq 2\pi$  are the polar angles measured from z-axis and x-axis, respectively, see Fig. 21. This emergent ray intersects the free water surface at a point P (see Fig. 21) represented by the vector  $\vec{P} = XP = (x_P, y_P, f(x_P, y_P))$ . Note that  $x_P \neq x, y_P \neq y$  because the projection of point P on the bottom does not coincide with X. In order to obtain the coordinates of P we write this vector beginning from origin to X and then along the emergent ray unit vector  $\vec{e}$ , that is

$$\vec{P} = \vec{X} + \lambda \vec{e},$$

where  $\lambda$  is a parameter given by the solution of the equation:

$$\lambda \cos \theta = f(x + \lambda \sin \theta \cos \varphi, y + \lambda \sin \theta \sin \varphi),$$

which is the condition for the emergent beam to intersect the water surface at point P. From now we denote the solution of the transcendental equation above by  $\lambda_1$  because this solution depends on the independent parameters of the problem, that is  $\lambda_1 = \lambda_1(x, y, \theta, \varphi)$ . This equation can be solved only numerically, even for the simplest surfaces. With  $\lambda_1$  thus calculated we can write the expressions of the coordinates of point P:

$$\begin{cases} x_P = x + \lambda_1 \sin \theta \cos \varphi \\ y_P = y + \lambda_1 \sin \theta \sin \varphi \\ z_P = f(x_P, y_P) \end{cases}$$

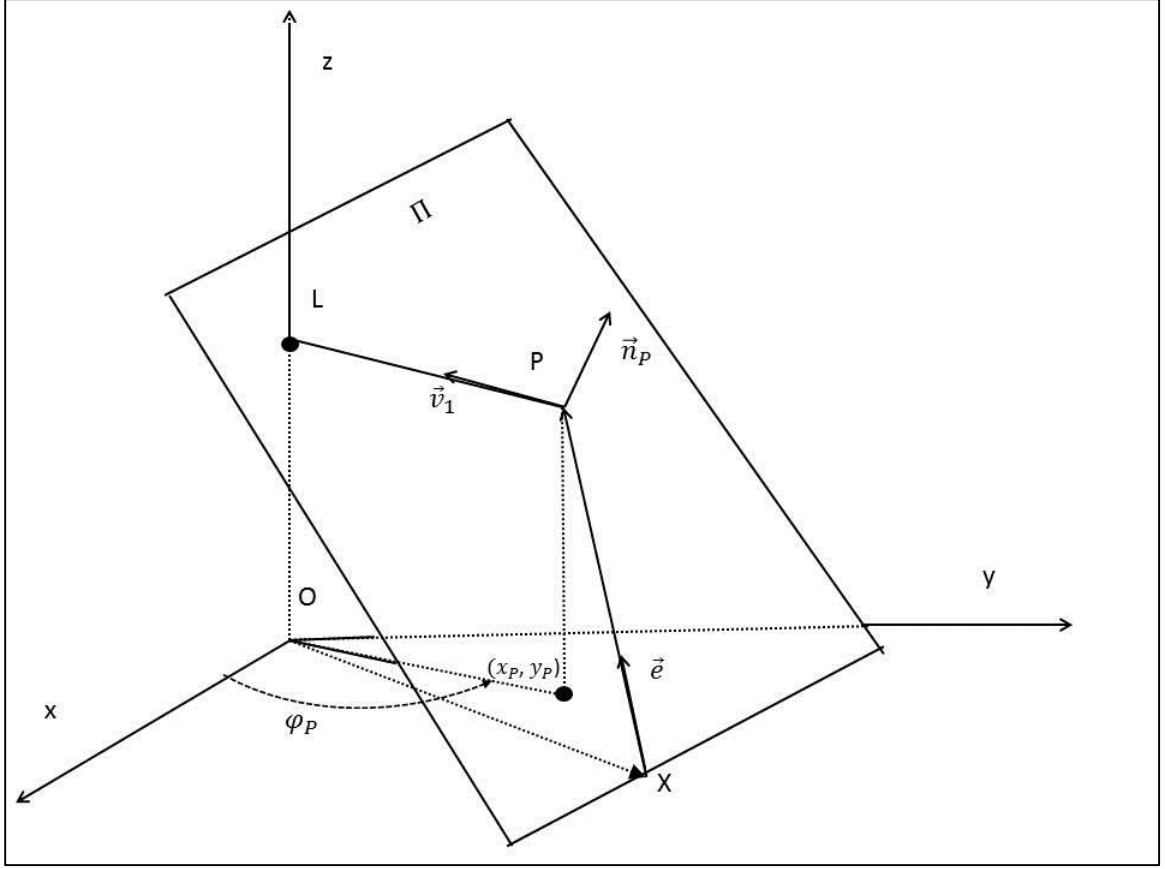


Fig. 21: Diagram of vectors for the full 3-dimensional calculations

We denote by  $\vec{n}_P$  the unit normal to the free surface at P, oriented upwards, see Fig.

21:

$\vec{n}_P$

$$= \left( -\frac{\frac{\partial f}{\partial x}}{\sqrt{\left(\frac{\partial f}{\partial x}\right)^2 + \left(\frac{\partial f}{\partial y}\right)^2 + 1}}, -\frac{\frac{\partial f}{\partial y}}{\sqrt{\left(\frac{\partial f}{\partial x}\right)^2 + \left(\frac{\partial f}{\partial y}\right)^2 + 1}}, -\frac{1}{\sqrt{\left(\frac{\partial f}{\partial x}\right)^2 + \left(\frac{\partial f}{\partial y}\right)^2 + 1}} \right),$$

where the derivatives of  $f$  are evaluated at  $(x_P, y_P)$  so the unit normal is a function  $\vec{n}_P = \vec{n}_P(x_P, y_P)$ . The emergent beam  $XP$  exits the water surface according to Snell's laws. Let the unit vector of this ray be  $\vec{v}$ ,  $\|\vec{v}\| = 1$ . According the Snell's first law the incident beam  $XP$ , the normal  $\vec{n}_P$  and the emergent out of water ray belong to the same



plane. We call this plane  $\Pi$ , and we know it is generated by the unit vectors  $\{\vec{e}, \vec{n}_p\}$ .

Hence, we can express the emergent ray coming out of water by:

$$\vec{v} = \frac{\vec{e} + \gamma \vec{n}_p}{\sqrt{1 + \gamma^2 + 2\gamma \vec{e} \cdot \vec{n}_p}},$$

where  $\gamma < 0$  (to insure the upwards direction of the final emergent ray) is a free parameter, See Fig. 21. In the following we make the notation  $\xi = \vec{e} \cdot \vec{n}_p$ . Snell's second law asks

$$\frac{\sin(\widehat{\vec{e}, \vec{n}_p})}{\sin(\widehat{\vec{v}, \vec{n}_p})} = \frac{1}{n},$$

where  $n$  is the water refraction index, and the hat represents the angle between the two vectors under hat. By introducing the above expressions for  $\vec{v}$ ,  $\gamma$  and  $\xi$  in the 2nd Snell's law we obtain the condition:

$$n^2 = \frac{\gamma^2}{1 + \gamma^2 + 2\gamma\xi}$$

For given values for  $n$  and  $\xi$  this equation has always two negative two solutions for  $\gamma$ , but only one (the largest in absolute value) is the physical one. We will denote this solution for the above equation by

$$\gamma \rightarrow \gamma_1 = -\xi + \frac{\sqrt{1 - n^2(1 - \xi^2)}}{n} < 0.$$

We introduce  $\gamma_1$  value for  $\gamma$  in the general expression for  $\vec{v}$  from above and obtain the correct emergent direction out of water, denoted  $\vec{v}_1$ :

$$\vec{v}_1 = \frac{\vec{e} + \left( \frac{\sqrt{1 - n^2(1 - \xi^2)}}{n} - \xi \right) \vec{n}_p}{\sqrt{1 + \left( \frac{\sqrt{1 - n^2(1 - \xi^2)}}{n} - \xi \right)^2 + 2\xi \left( \frac{\sqrt{1 - n^2(1 - \xi^2)}}{n} - \xi \right)}}$$

with  $\vec{v}_1$  still normalized.

This unit vector  $\vec{v}_1$  should be extended to the lens point, L, see Fig. 21. So we are going to multiply this unit vector with an arbitrary parameter  $\mu$ , and determine the value of this parameter from the condition:

$$(\vec{P} + \mu\vec{v}_1)_z = H,$$

that is the z-component of the vector  $\text{OX} + \text{XP} + \text{PL} = \text{OL}$  is the height of the lens.

There is an additional condition which will determine the angles  $\theta, \varphi$  of the initial bottom emergent ray to end into the lens, namely:

$$\left[ (\vec{P} + \mu\vec{v}_1)_x \right]^2 + \left[ (\vec{P} + \mu\vec{v}_1)_y \right]^2 \leq R,$$

That is the final emergent ray PL must collide the inside of the disk of radius R, which represents the front lenses of the camera. We will use this inequality to obtain the domain of variation of the angles  $\theta, \varphi$  emerging from X such that the rays will enter the lenses. In optic this locus is called the caustic surface of point X through the water refracting medium, see Burkhard (1973).

By introducing the expression of  $\vec{P}$ , and  $\vec{v}_1$  in the vertical matching condition  $(\vec{P} + \mu\vec{v}_1)_z = H$ , we obtain the final value of parameter  $\mu$  which we call  $\mu_1$ ;

$$\mu_1 = \frac{(H - \lambda_1 \cos \theta) \sqrt{1 + \gamma_1^2 + 2 \gamma_1 \xi}}{\cos \theta + \frac{\gamma_1}{\sqrt{\left(\frac{\partial f}{\partial x}\right)^2 + \left(\frac{\partial f}{\partial y}\right)^2 + 1}}},$$

where the derivatives of f are again calculated at  $(x_p, y_p)$ ,  $\lambda_1$  is the solution described above, and  $\xi$  has the same signification of dot product. In Fig. 21 we present all the vectors  $\vec{e}$ ,  $\text{XP} = \lambda_1 \vec{e}$ ,  $\vec{n}_p$ , and  $\mu_1 \vec{v}_1$  described above, all belonging to the same

plane  $\Pi$ . The sequence of vectors  $\text{OX}+\text{XP}+\text{PL}$  take the origin into the bottom pattern reference point X, to the impact with water point P, and out of water to the lens L.

The procedure in the following consists in 2 steps.

Step 1. Given  $(x,y)$  we calculate all the parameters in the system, namely  $\{x_P, y_P, \lambda_1, \xi, \gamma_1, \mu_1\}$  for these  $x, y$  and in general for all values of the angles  $\theta, \varphi$ .

Next, solve the “center equation”

$$\begin{cases} (\vec{P} + \mu\vec{v}_1)_x = 0 \\ (\vec{P} + \mu\vec{v}_1)_y = 0' \end{cases}$$

This equation requests that the final emergent ray P to arrive into the center of the lens L of coordinates  $(0, 0, H)$ . These two equations, highly nonlinear and transcendental can be solved only numerically and will provide those values (denoted  $\theta_L, \varphi_L$ ) for the angles  $\theta, \varphi$  for which the ray generated at X ends up at center of L.

These two equations have the following explicit forms:

$$\left\{ \begin{array}{l} x + \lambda_1 \sin \theta_L \cos \varphi_L + \frac{\mu_1}{\sqrt{1 + \gamma_1^2 + 2 \gamma_1 \xi}} \left( \sin \theta_L \cos \varphi_L - \frac{\gamma_1 \frac{\partial f}{\partial x}}{\sqrt{\left(\frac{\partial f}{\partial x}\right)^2 + \left(\frac{\partial f}{\partial y}\right)^2 + 1}} \right) = 0, \\ y + \lambda_1 \sin \theta_L \sin \varphi_L + \frac{\mu_1}{\sqrt{1 + \gamma_1^2 + 2 \gamma_1 \xi}} \left( \sin \theta_L \sin \varphi_L - \frac{\gamma_1 \frac{\partial f}{\partial y}}{\sqrt{\left(\frac{\partial f}{\partial x}\right)^2 + \left(\frac{\partial f}{\partial y}\right)^2 + 1}} \right) = 0 \end{array} \right.$$

Step 2. Having the central ray PL into the center of the lens, we rely on the smallness of the lens radius compared to the heights of lens and water, and to the mean values of the bottom patterns, that is  $R \ll h, H, L_x, L_y$ . Under this “geometrical optics”

approximation we consider that the rest of the rays entering into the lens are just infinitesimal variations  $\delta\theta, \delta\varphi$  around  $\theta_L, \varphi_L$  respectively.

Coming back to the last level of calculations, we need to take the final emergent ray PL and pass it through the lens onto the camera sensor plane. We assume that the camera sensor plane is also horizontal, centered at z-axis and we overlap on it the same x, y coordinates. According to the same “geometric optics” approximation we assume that the final images of pattern points X will be projected onto the focal plane of the camera, so we neglect at this point the fuzziness generated by miss-focusing. The ray PL enters the lenses at an angle  $\Phi$  made with the z-axis given by  $\cos \Phi = |(\vec{v}_1)_z|$ . This expression arises from the dot product between the unit vector  $\vec{v}_1$  and the z-axis unit vector.

The “central ray” enters the lens at the center (0,0,H) of the lens at angle  $\Phi$ , emerges through the lens at the same angle (geometric optics approximation) and intersects the focal plane at a point Q. This Q point has its z-coordinate  $Q_z = H + F$  (placed in the focal plane) and it is placed at a distance  $\rho$  from the z-axis. The PL ray is in the vertical plane  $\Pi$  that makes the angle  $\varphi_P$  with the x-axis, see Fig. 21. The ray exits the lens at the same angle  $\varphi_P$  with the x-axis, and ends at point Q. So the position of point Q is diametric opposed from point P, in the focal plane on a circle of radius  $\rho$ . Let  $(x_I, y_I, H + F)$  be the coordinates of Q (label I as in image). We have:

$$\begin{cases} x_I = \rho \cos \varphi_L \\ y_I = -\rho \sin \varphi_L \end{cases}$$

with  $\rho$  given from triangle similarity:

$$\rho = F \frac{\sqrt{1 - [(\vec{v}_1)_z]^2}}{|(\vec{v}_1)_z|}.$$

Gathering all these expressions in a final equation we have the position of the image of source object point X, onto the camera sensor in the focal plane given by:

$$\begin{cases} x_I = F \frac{\sqrt{1 - [(\vec{v}_1)_z]^2}}{|(\vec{v}_1)_z|} \frac{x_P}{\sqrt{(x_P)^2 + (y_P)^2}} \\ y_I = -F \frac{\sqrt{1 - [(\vec{v}_1)_z]^2}}{|(\vec{v}_1)_z|} \frac{y_P}{\sqrt{(x_P)^2 + (y_P)^2}} \end{cases}$$

These last equations represent the final result of this fully 3-dimensional model. Namely, from an object point X at the bottom, we calculate all the parameters such that the final emergent ray PL arrives at the center of the lenses, that is find  $\theta_L$  and  $\varphi_L$ . The image of the point X is given by the above final equations, in the focal plane, Next step, we differentiate the above equations with respect to  $\theta$ ,  $\varphi$ , and  $\lambda$  and linearize them to the first order of differentiation around the center values  $\theta_L$  and  $\varphi_L$ . To do this we have to perform an intermediate step: differentiate the equation for  $\lambda_1$  (see it above):

$$\lambda \cos \theta = f(x + \lambda \sin \theta \cos \varphi, y + \lambda \sin \theta \sin \varphi),$$

with respect to  $\theta$ ,  $\varphi$ , and  $\lambda$  and find a relation between the derivatives  $\frac{\delta\lambda}{\delta\theta}$ , and  $\frac{\delta\lambda}{\delta\varphi}$ . Next, we substitute the  $\lambda$  derivatives in the linearized expression for  $x_I, y_I$  and

transform the above equalities in the inequality  $\left[ (\vec{P} + \mu\vec{v}_1)_x \right]^2 + \left[ (\vec{P} + \mu\vec{v}_1)_y \right]^2 \leq R$ .

This inequality will set the limiting values to  $\delta\theta$ ,  $\delta\varphi$ . This will give the maximal cone of light emerging from X which is completely absorbed by the lens. The differentials  $dx_I, dy_I$  will provide the size and shape of the spot of light into which the object point X is mapped.

We performed all these calculations for the test sine wave function presented at the beginning of this section. We evaluate the position of the image points  $x_I, y_I$  in the

focal plane based on the above calculations. Then we performed experiments in the wave tank and generate similar sine wave and take snap shots of their image in the camera. Finally we compared the calculations with the experiment and obtain a satisfactory result.

In the figure below we show few typical sine waves generated in the wave tank:



Figure 22: Sine wave Generator

In the following picture we show the bottom pattern grid used for reference (the corners of the squares were positions X from the calculations):



Figure 23: Grid placement inside the tank

The height of the real waves was determined with 4 capacitive gauges placed in (the vertical metal rods in the figures). The data from the capacitive level gauges were double checked with photos from the AOS rapid camera at 1,000 frames/second:

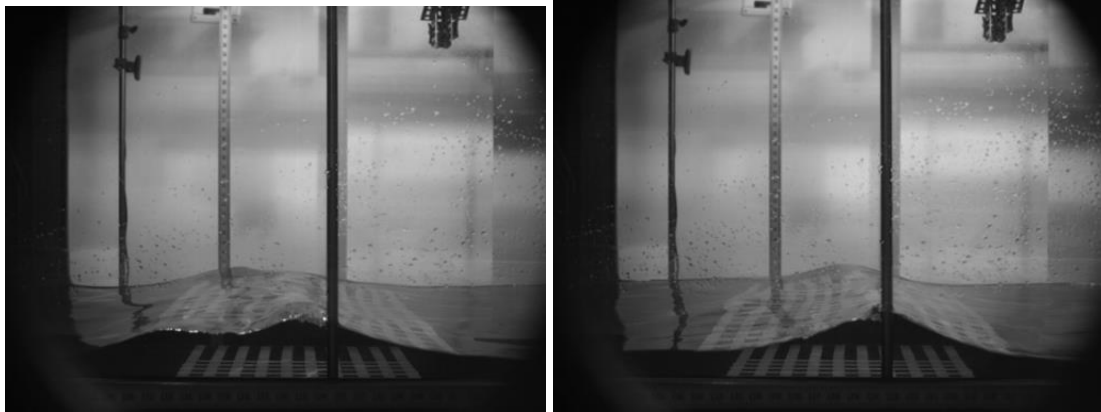


Figure 24: Waves captured using high speed camera.

The image of the chess-board was obtained by placing a regular Cannon camera on the top of the free water surface. Here below are presented two typical images when sine waves pass over the chess-board:

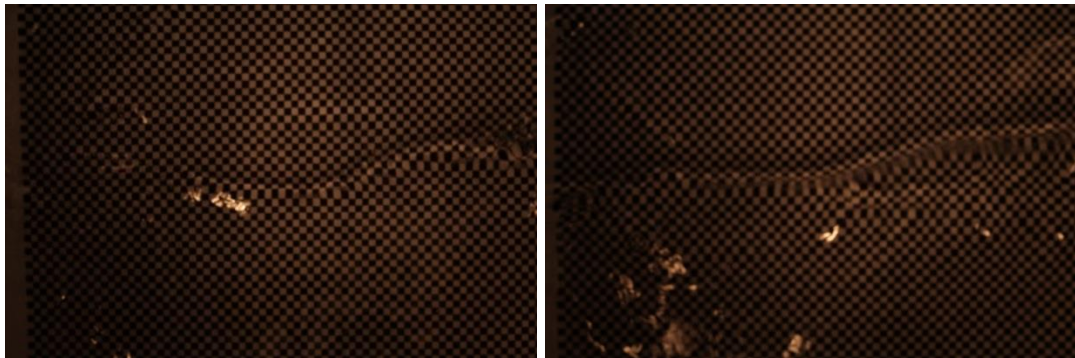


Figure 25: Overhead view of sine wave passing over the grid

The signal from the capacitive level gauges was processed by a Tektronix memory oscilloscope:

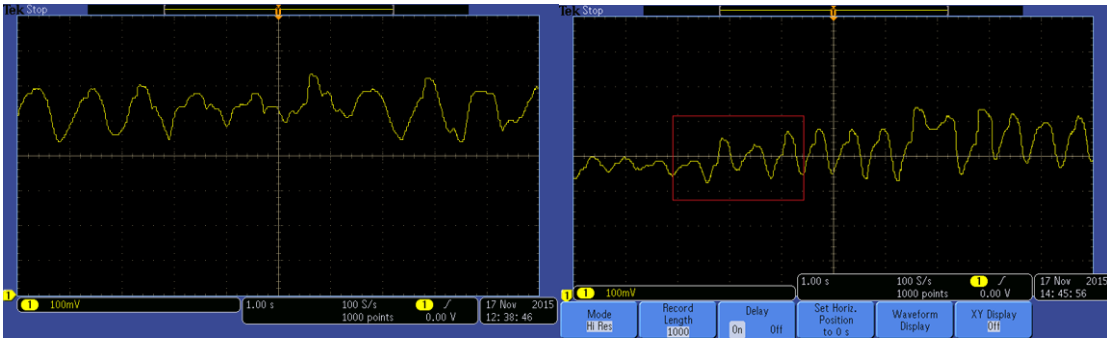


Figure 26: Height measured using oscilloscope

In the figures below we present the final analysis of data and comparison with experiments. We compare here the signal from level gauges, with the digitized image from the rapid camera, and with the numeric simulation presented in this thesis for most regular sine waves we could obtained:

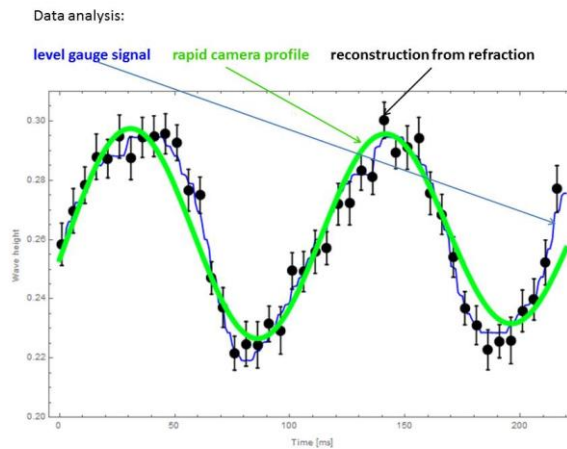


Figure 27: Comparison of heights using numerical method rapid camera and level gauges

In the figure below we present the same quantities for a more irregular wave profile:



The method applied to a more irregular wave profile:

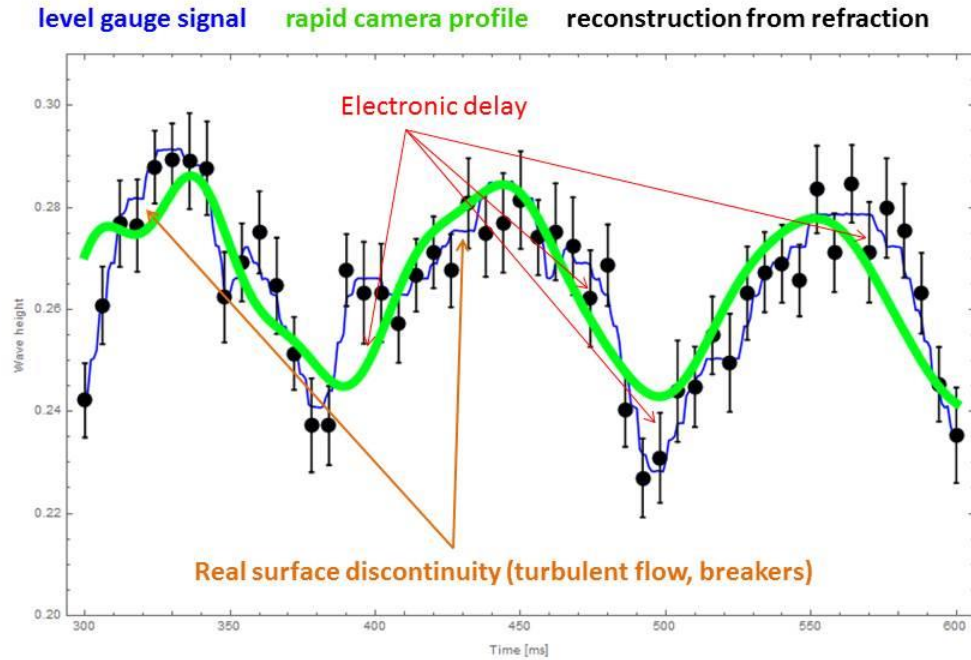


Figure 28: Irregular waves compared using the three listed methods

We notice a pretty good matching between experiment and theory. The deviation between the rapid camera data and the measured/calculated data can be explained by a random electronic delay of the signal.

From these results we can draw the following conclusions:

The image in the camera tends to become defocused if the wave has too high amplitude or is too steep. Different points in the same plane need to focus in different image planes.

From the above complicated/nonlinear equations we know that the object-to-image transformation is not one-to-one, so that different object points can merge in the same image point. This explains why the image appears sometimes broken. This effect

happens when the height of the waves is too large, or the camera too close and the geometric optic approximation is not valid anymore.

Illumination should be carefully chosen to eliminate all parasite reflections on wavy water surface that cannot be predicted from horizontal surface.

The system always needs at least one level gauges to measure the average height of the wave at one point.

The major advantages of our method are 2: It is fully 3-dimensional procedure, and it is able to reconstruct the wave field simultaneously over all the investigated area, hence it may render good data for tsunami prevention. In addition our method is easy to calibrate and to use.

## Chapter 6: Summary and conclusion

The investigators begin the research with the concept that an object under water will change in magnification with change in the height of the water in which the object is placed when observed by a camera or observer outside water.

The study led to the derivation of a novel equation to calculate the apparent height of an object with the change in water levels or change in the distance of the object from the center of origin of the camera.

The equations were simulated in MATLAB for various test cases and the results obtained were in section 4 and compare them to the initial results obtained using Mathematica Appendix C.

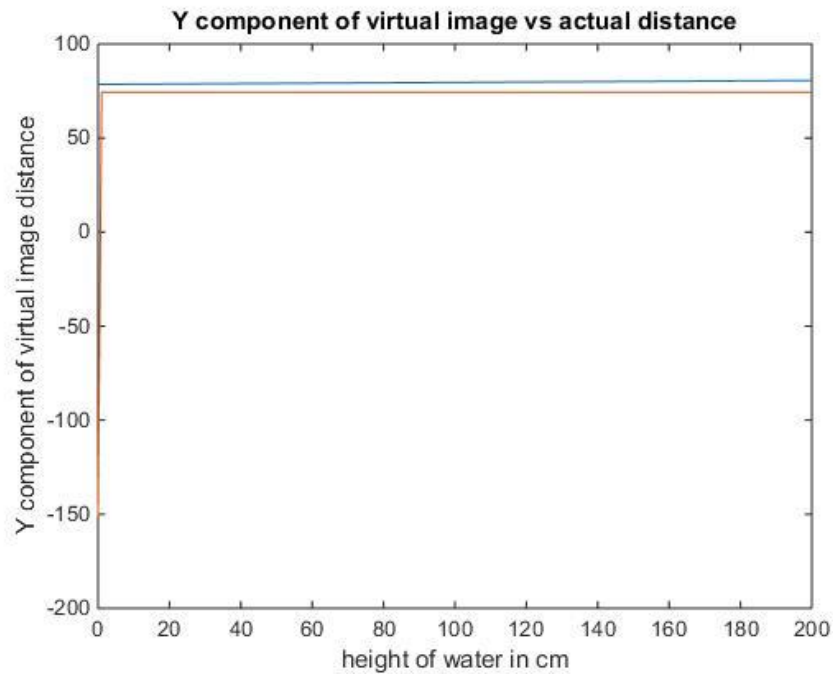


Figure 29: Y component Vs Water height.

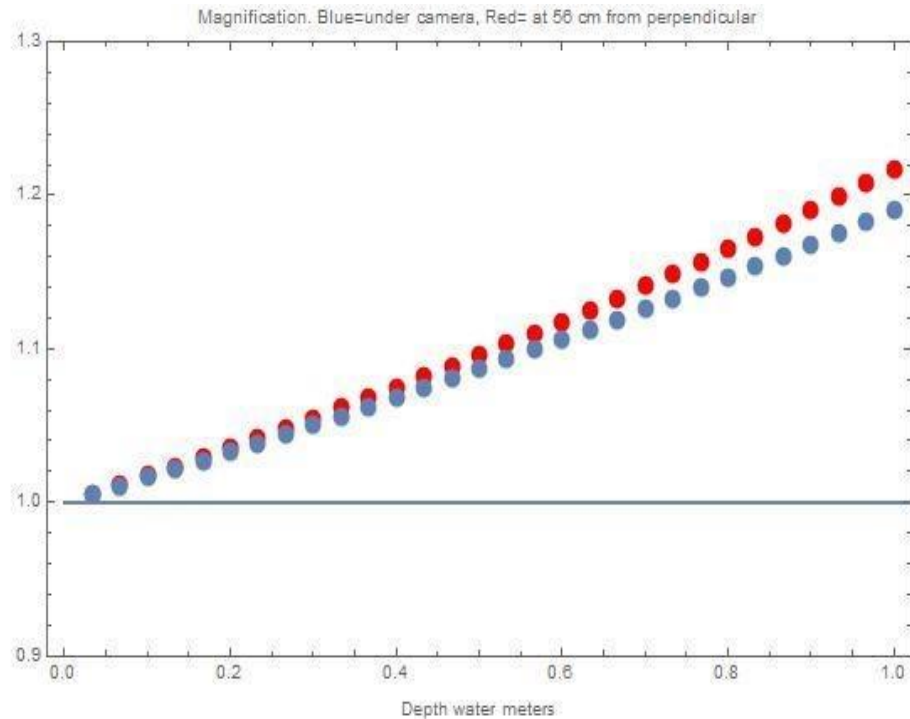


Figure 30: The Predicted result Using Mathematica [Appendix C]

It is seen from the above figures that the change in water height leads to the apparent change in height of the object. This can be identified as apparent magnification of the object thus confirming that change in water height impacts the magnification of objects seen in water.

The same is seen when the water is slightly inclined to the steady surface as seen in section 3.2. These concepts can be used to further the study of water waves thus a stepping stone to Tsunami warning system.

Another concept to measure the height of water by comparing images distorted by water to the restored and reconstructed images is mentioned. Hence a brief study is done in reconstruction of images under water.

## Conclusion

The main purpose of the research is to express the relation of water height to magnification of objects under water. The relation derived is than tested at different cases to further strengthen the argument that change in water height leads to apparent change in magnification of the object under water to a certain extent.

This research is a stepping stone to building a fool-proof tsunami warning system which could help save thousands of lives and mitigate damage caused by tsunamis.

At the beginning, the task first at hand was to check the delay the images were captured simultaneously between the two stereo cameras. The physical setup was constructed fairly quickly and testing can be done smoothly. Next the investigators clicked images to have a practical idea of whether the images under water have any apparent magnification with increase in water height. Though the images showed magnification on physical calculation, implementing an initial software program to calculate it for various water heights had a serious drawback.

Firstly, on adding every inch of water in the tank, the images were extremely distorted due to the following reasons:

- The distortion from images due to water increased exponentially with every inch of water added.
- After about 5 inches of water, without an external source of light the image was impossible to capture since the object would be extremely darkened to get any useful info out of it.
- The use of external lights was suggested but due to the refractive and reflective properties of water, it could add only a few more inches to the water before image distortion.
- The suggestion of image restoration and correction was suggested to then further process the distorted images and compare magnification, but image correction led to change in the original image characteristics which would affect the comparison of magnification significantly since the change is very minute.

Hence the calculation for magnification was done physically as shown in images below.



Figure 31: Image of a coin with no water



Figure 32: Image of the same coin with 1 inch water added.

We see that with every inch the magnification was approximately equal to the refractive index of water.

Next, the mathematical equation derived were tested using MATLAB. In the end, research is conducted in image reconstruction to solve the problem of image distortion and surface reconstruction.

## **Future Work**

The Investigators have given a mathematical approach to change in magnification of objects under water with change in water height. Future research would include demonstration and comparison of original and images with increased water height using a software to back up the current research.

The study compares various image restoration and surface reconstruction methods which can be researched further and implemented for better results. Also the above study could help in processes like Dredging which is very important in countries where ore transport and other forms of water transport is prominent.

The mathematical approach shown above is for steady waves and waves at smaller angles. Further study is to be conducted for waves of different shapes and heights.

## References

- [1] Yuandong Tian and Srinivasa G. Narasimhan, "Seeing through Water: Image Restoration using Model-based Tracking". Proc. of IEEE International Conference of Computer Vision (ICCV), Oct, 2009.
- [2] Douglas Enright, Ronald Fedkiw, Joel Ferziger, and Ian Mitchell. A hybrid particle level set method for improved interface capturing. In Proceedings of SIGGRAPH 2002, ACM Press / ACM SIGGRAPH, 2002.
- [3] Nick Foster and Ronald Fedkiw. Practical animation of liquids. In Proceedings of SIGGRAPH 2001, ACM Press / ACM SIGGRAPH, pages 23–30, 2001.
- [4] Nick Foster and Dimitri Metaxas. Realistic animation of liquids. In Graphical models and image processing, 1995.
- [5] H. Murase, Surface Shape Reconstruction of a Nonrigid Transparent Object Using Refraction and Motion. IEEE Transactions on Pattern Analysis and Machine Intelligence, Vol. 14, No. 10, Oct 1992
- [6] S.Ullman, The Interpretation of Visual Motion. Cambridge, MA: MIT press,1979.
- [7] Michael Kass and Gavin Miller. Rapid, stable fluid dynamics for computer graphics. In Proceedings of SIGGRAPH 1990, ACM Press / ACM SIGGRAPH, pages 49–55, 1990.
- [8] D. Peachy. Modeling waves and surf. In Proceedings of SIGGRAPH 1986, ACM Press / ACM SIGGRAPH, pages 65–74, 1986.
- [9] Bernd J`ahne, Jochen Klinke, and Stefan Waas. Imaging of short ocean wind waves: a critical review. Journal of Optical Society of America, 11(8):2197–2209, 1994.
- [10] Bernd J`ahne, Jochen Klinke, Peter Geissler, and Frank Hering. Image sequence analysis of ocean wind waves. In Proceedings of the International Seminar on Imaging in Transport Processes, 1992.
- [11] O.H. Shemdin. Measurement of short surface waves with stereophotography. In Engineering in the Ocean Environment. Conference Proceedings, pages 568–571, 1990.
- [12] Xin Zhang and Charles Cox. Measuring the two-dimensional structure of a wavy water surface optically: A surface gradient detector. Experiments in Fluids, Springer Verlag, 17:225–237, 1994.
- [13] Hiroshi Murase. Shape reconstruction of an undulating transparent object. In Proc. IEEE Intl. Conf. Computer Vision, pages 313–317, 1990.



[14] Nigel Jed Wesley Morris. Image-based Water Surface Reconstruction with Refractive Stereo, Graduate Department of Computer Science, University of Toronto, 2004

[15] W. C. Keller and B. L. Gotwols. Two-dimensional optical measurement of wave slope. *Applied Optics*, 22(22):3476–3478, 1983.

[16] J.M. Daida, D. Lund, C. Wolf, G.A. Meadows, K. Schroeder, J. Vesecky, D.R. Lyzenga, B.C. Hannan, and R.R. Bertram. Measuring topography of small-scale water surface waves. In *Geoscience and Remote Sensing Symposium. Conference Proceedings*, volume 3, pages 1881–1883, 1995.

[17] Ludu, Andrei, Final. Laser, Daytona Beach, FL, Embry-Riddle Aeronautical University. 2012

[18] Nejad, Sh. Mohammed and M. H. Haji Mirsaeidi, Altitude Measurement using Laser Beam Reflected from Water Surface, *Iranian Journal of Electrical & Electronic Engineering*. 2005

[19] Ladyada, Photoconductive Cells,  
[http://www.ladyada.net/media/sensors/APP\\_PhotoCellIntroduction.pdf](http://www.ladyada.net/media/sensors/APP_PhotoCellIntroduction.pdf). 2012

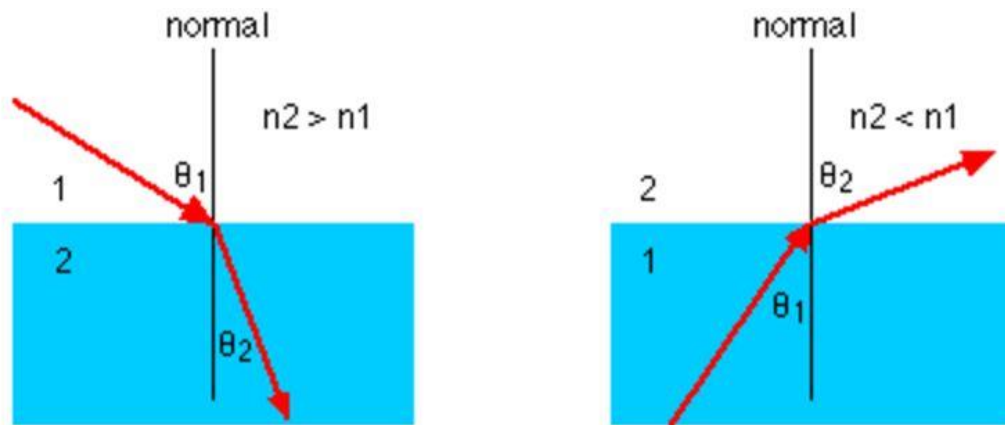
[20] NOAA, Triaxys Directional Wave Buoy for Nearshore Wave Measurements – Test and Evaluation Plan, <http://tidesandcurrents.noaa.gov/publications/techrpt38.pdf>. 2003

[21] Burkhard, D. G., and Shealy, D. L., Flux density for ray propagation in geometrical optics, *Optical Society of America*, 63, 3 (1973) 299-304.

## Appendix A Snell's Law

The bending of path of a light wave as it traverses from one medium to another is known as Refraction. This occurrence is seen at the intersection of the two mediums in question and caused due to the change in speed of the light wave upon crossing the boundary. The ray of light bends in one direction or another depending upon whether the ray of light speeds up or slows down at the juncture of the two materials.

The speed of light depends on the optical density of the medium it is traversing through. The Example below will illustrate the principle more clearly.



Snell's law :  $n_1 \sin\theta_1 = n_2 \sin\theta_2$  or, equivalently,  $\sin\theta_1 / \sin\theta_2 = v_1 / v_2$

Fig. Illustration of Snell's law.

<http://www.eserc.stonybrook.edu/projectjava/snell/>

If a ray of light passes across a medium in which it travels fast into one that travels slower, then the light ray will bend towards the normal line i.e. when refractive index [R.I.] of the first medium  $n_1$  is less than the refractive index of the second  $n_2$ .

Similarly, if the ray of light is travelling from a medium of higher R.I.  $n_2$  to lower R.I.  $n_1$  than we see that the ray of light bends away from the normal.

Critical angle: when the refracted ray makes an angle of 90 degrees to the normal, the angle is called Critical angle. If the ray makes an angle higher than 90 than we say Total Internal Reflection [T.I.R] has occurred. T.I.R. is illustrated below.

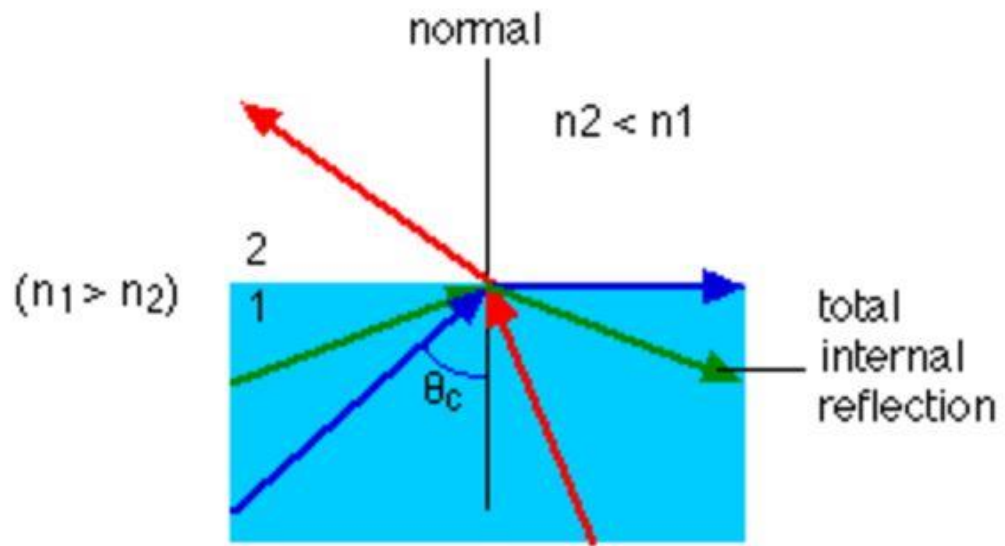


**Fig : Illustration of T.I.R.**

## Appendix B Matlab Codes

```
clear
clc
%% Setting up initial parameters for the experiment
n = 1.33; %Refractive index of water
x = 50;
h = 0:0.01:2; % Height of water surface
H = 3-h; % height of camera from water
L = 5; % Aperture of camera in cm
%% Iteration to calculate values based on equation
%for i= 1:length(x)
i=1;
for j = 1:length(h)
    syms b
    %eq1 = sin(b)/sqrt(1-(sin(b)^2))+(20*sin(b))/sqrt(1-n*sin(b)^2)+10-
x(i);

    eqn_beta = h(j)*vpa(tan(b))+ (H(j)*vpa((sin(b)))/vpa(sqrt(1-
n*vpa(sin(b)^2))))- L/2 == x;
    eqn_beta = vpa(eqn_beta);
    solution_beta(i,j) = double(solve(eqn_beta,b));

    eqn_alpha = h(j)*vpa(tan(b))+ (H(j)*vpa((sin(b)))/vpa(sqrt(1-
n*vpa(sin(b)^2))))+ L/2 == x;
    eqn_alpha = vpa(eqn_alpha);
    solution_alpha(i,j) = double(solve(eqn_alpha,b));

    % DISREGARDING NEGATIVE VALUES OF BETA, ALPHA SINCE TIR angle is 90
    % degrees and all values out of this range can be ignored.
    if solution_beta(i) < 0
        solution_beta(i) = 0;
    end
    if solution_alpha(i) < 0
        solution_alpha(i) = 0;
    end
end
%end

%% Calculate Alpha' and Beta'
solution_alpha_dash = asin(n*sin(solution_alpha));
solution_beta_dash = asin(n*sin(solution_beta));

%% Calculate Y component
syms y
for i = 1:length(h)
    eqn_y = h(i) + H(i) - (L/(tan(solution_beta_dash(i)) -
tan(solution_alpha_dash(i)))) == y;
    y_dash(i) = solve(eqn_y,y);
end

%% Calculate X component
syms z
for i = 1:length(h)
```

```

    eqn_z =
    (L/2)+((L*tan(solution_alpha_dash(i)))/(tan(solution_beta_dash(i)) -
tan(solution_alpha_dash(i)))) == z;
    z_dash(i) = solve(eqn_z,z);
end

%% Plotting

solution_beta_dash_deg = solution_beta_dash*180/pi;
solution_alpha_dash_deg = solution_alpha_dash*180/pi;

figure(1),plot(h,solution_beta_dash_deg)
title('Beta dash angle versus object distance from camera')
xlabel('height of water in cm')
ylabel('Angle in degrees')
figure(2),plot(h,solution_alpha_dash_deg)
title('Alpha dash angle versus object distance from camera')
xlabel('height of water in cm')
ylabel('Angle in degrees')
hold on;
figure(3), plot(h,y_dash)
title('Y component of virtual image vs actual distance')
xlabel('height of water in cm')
ylabel('Y component of virtual image distance')

hold on;
figure(4), plot(h,z_dash)
title('X component of virtual image vs actual distance')
xlabel('height of water in cm')
ylabel('X component of virtual image distance')

hold on;

n =1.33; %Refractive index of water
x = 0;
h = 0:0.1:2; % Height of water surface
H = 3-h; % height of camera from water
L = 5; % Aperture of camera in cm
%% Iteration to calculate values based on equation
%for i= 1:length(x)
i=1;
for j = 1:length(h)
    syms b
    %eq1 = sin(b)/sqrt(1-(sin(b)^2))+ (20*sin(b))/sqrt(1-n*sin(b)^2)+10-
x(i);

    eqn_beta = h(j)*vpa(tan(b))+ (H(j)*vpa((sin(b)))/vpa(sqrt(1-
n*vpa(sin(b)^2))))- L/2 == x;
    eqn_beta = vpa(eqn_beta);
    solution_beta(i,j) = double(solve(eqn_beta,b));

    eqn_alpha = h(j)*vpa(tan(b))+ (H(j)*vpa((sin(b)))/vpa(sqrt(1-
n*vpa(sin(b)^2))))+ L/2 == x;
    eqn_alpha = vpa(eqn_alpha);
    solution_alpha(i,j) = double(solve(eqn_alpha,b));

```

```

% DISREGARDING NEGATIVE VALUES OF BETA, ALPHA SINCE TIR angle is 90
% degrees and all values out of this range can be ignored.
if solution_beta(i) < 0
    solution_beta(i) = 0;
end
if solution_alpha(i) < 0
    solution_alpha(i) = 0;
end
end
%end

%% Calculate Alpha' and Beta'
solution_alpha_dash = asin(n*sin(solution_alpha));
solution_beta_dash = asin(n*sin(solution_beta));

%% Calculate Y component
syms y
for i = 1:length(h)
    eqn_y = h(i) + H(i) - (L/(tan(solution_beta_dash(i)) -
tan(solution_alpha_dash(i)))) == y;
    y_dash(i) = solve(eqn_y,y);
end

%% Calculate X component
syms z
for i = 1:length(h)
    eqn_z =
(L/2)+((L*tan(solution_alpha_dash(i)))/(tan(solution_beta_dash(i)) -
tan(solution_alpha_dash(i)))) == z;
    z_dash(i) = solve(eqn_z,z);
end

hold on;
figure(3), plot(h,y_dash)
title('Y component of virtual image vs actual distance')
xlabel('height of water in cm')
ylabel('Y component of virtual image distance')

hold on;
figure(4), plot(h,z_dash)
title('X component of virtual image vs actual distance')
xlabel('height of water in cm')
ylabel('X component of virtual image distance')

hold on;

```

## Appendix C Mathematica Simulation And Theory

Calculations:

Fig. 1 General diagram of objects, images, light rays.

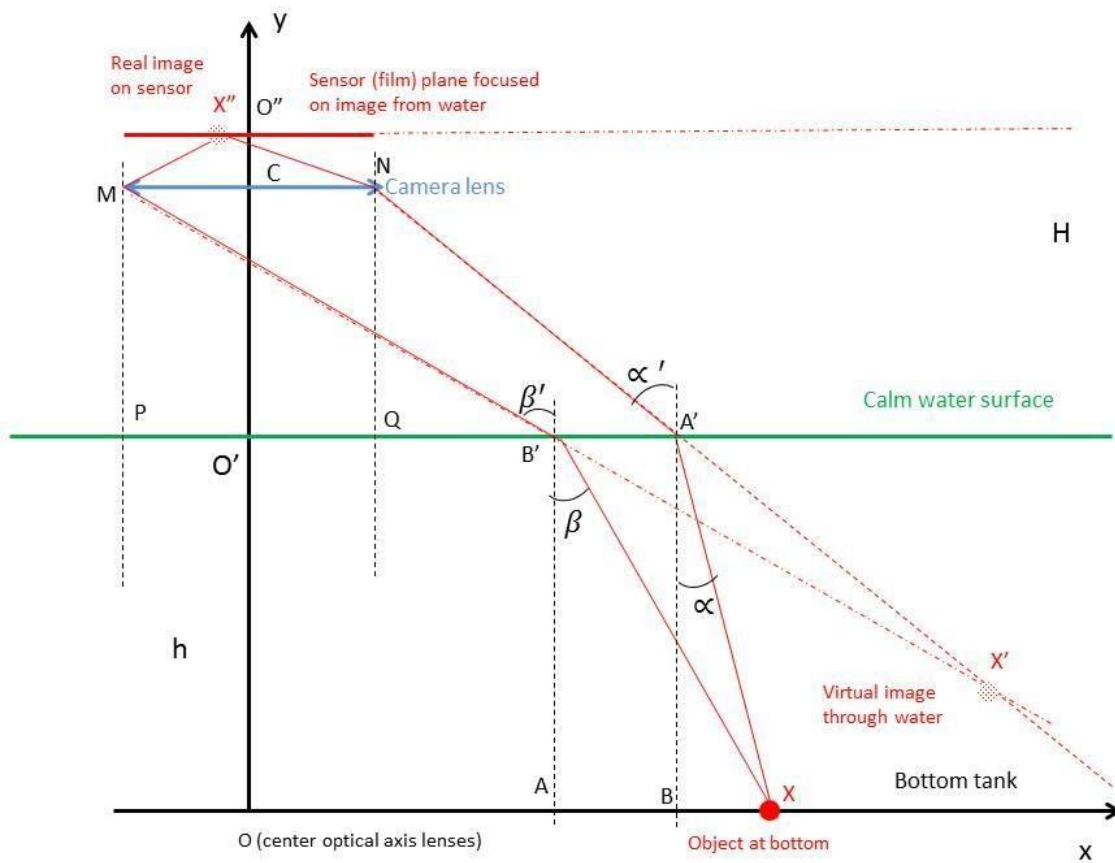


Fig. 1 Diagram of experiment, light rays, object and images

Explanation Fig. 1: An object X (red color) is placed on bottom (black thick horizontal line, also x-axis) at distance x from the foot O of the perpendicular  $CO'O$  from the lens of camera MN (blue horizontal line, of optical center C).

Vertical  $OO'CO''$  is also y-axis. Calm water (green horizontal line) of depth  $O'O=h$ . The lens has diameter  $MN=L$  and center C. Distance lens-water  $CO'=H$ . The sensor (photographic film) plane is the upper red horizontal line through point  $O''$ .

We send from the object X all light rays upwards towards water surface. The light received by the camera through its lens MN is only bounded by rays XB' and XA'.

These rays refract at water surface and become B'M and A'N, and anything between them enters into the lens. These two rays go through camera lens and focus on the final image on camera sensor X''. We assume the lenses is focused such that the sensor plane is exactly in X'' and the image is sharp.

Angles between normal to water at B' are  $\beta$  and  $\beta'$  and at A' are  $\alpha$  and  $\alpha'$  and we have Snell's relations  $\sin \alpha' = n \sin \alpha$ ,  $\sin \beta' = n \sin \beta$ .

Given and fixed are the quantities: n, x, h, H, L and f the focal distance of the lenses.

From the geometry we find the equation relating the angles with x:

$$H \frac{n \sin \alpha}{\sqrt{1 - n^2 \sin^2 \alpha}} - \frac{L}{2} - x + h \tan \alpha = 0$$

$$H \frac{n \sin \beta}{\sqrt{1 - n^2 \sin^2 \beta}} + \frac{L}{2} - x + h \tan \beta = 0$$

These 2 relations are to be solved numeric and get  $\alpha$  and  $\beta$ , and then from Snell's relations  $\alpha'$  and  $\beta'$ .

The image actually "seen" by the camera is at X' because of the refraction through water. The image is virtual and it can be obtained by extending backwards the light rays MB' and NA' until they intersect at X'. So the object X forms a virtual image X' through water. The coordinates of this image X'(x,y) are given by:

$$\begin{aligned} \text{Component } x \text{ of } X' &= \\ &= \frac{L(L - H \tan \alpha' + H \tan \beta')}{2H(\tan \alpha' - \tan \beta')} \\ &+ \left(-\frac{L}{2} + H \tan \alpha'\right) \left(1 + \frac{L - H \tan \alpha' + H \tan \beta'}{H(\tan \alpha' - \tan \beta')}\right) \end{aligned}$$

Component y of X' =



$$- \frac{+ \quad - \quad \tan \alpha + \quad \tan}{(h \quad H)(L \quad H \quad ['] \quad H \quad \beta')} + h \left( 1 + \frac{- \quad \tan \alpha + \quad \tan}{L \quad H \quad ' \quad H \quad \beta'} \right)$$

where the angles depend on x as shown above.

Image X' becomes object for the lenses. The camera lenses map X' into a real image X'' on the film (sensor plane) in camera.

All in all the whole line OX on bottom is mapped in the line O''X'' on the camera sensor. By applying the lens formulas and the magnification formulas

$$\frac{1}{CO''} + \frac{1}{H + h - \text{Component } y \text{ of } X'} = \frac{1}{f}$$

$$\frac{1}{H + h - \text{Component } y \text{ of } X'} = \frac{1}{\text{Component } x \text{ of } X'}$$

so in the end we obtain the length of segment O''X'' as a function of x.

Let us denote O''X''=I, as in the length of the image. What we obtain is the function I=I(x; h,H,L,f,n) that is the length I of the image O''X'' function of the horizontal displacement of the object x, and the other parameters of the experiment.

In continuation we present the results of some Mathematica program runs on these formulas for 2 situations. For both situations we choose n=1.33, L=4cm, H=60cm, f=45mm and h=1m.

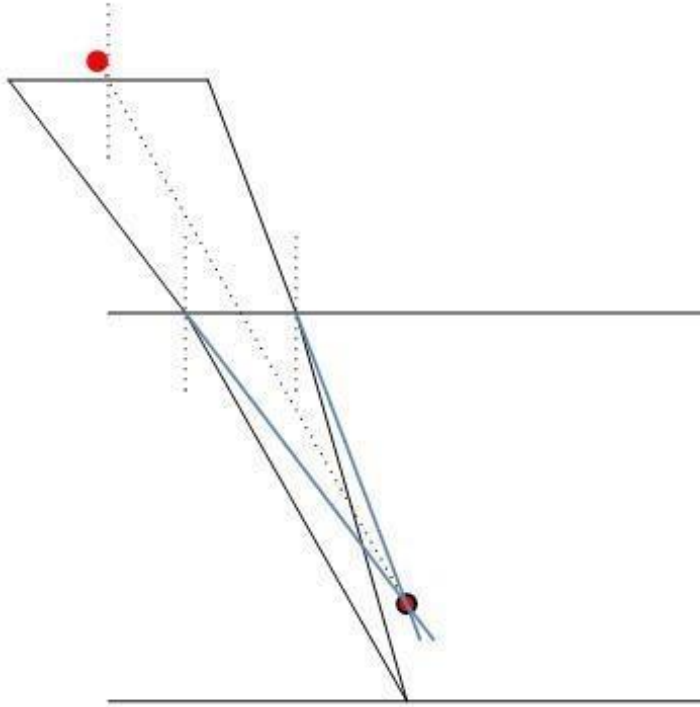


Fig. 2 The tip of the black inverted triangle is X where object is on bottom. The red spot with black contour is image through water, X'. The lowest black horizontal line is bottom, the next one is water surface and the last shorter horizontal line is the lens diameter. The top red spot is where final image of X, that is X'', forms on camera sensor plane. In this image  $x=6\text{cm}$ , that is just a little bit away ( $6-4/2=4\text{cm}$ ) from the perpendicular foot. Dotted lines show normal and the oblique dotted is the virtual-water-image X' to center of lens line.

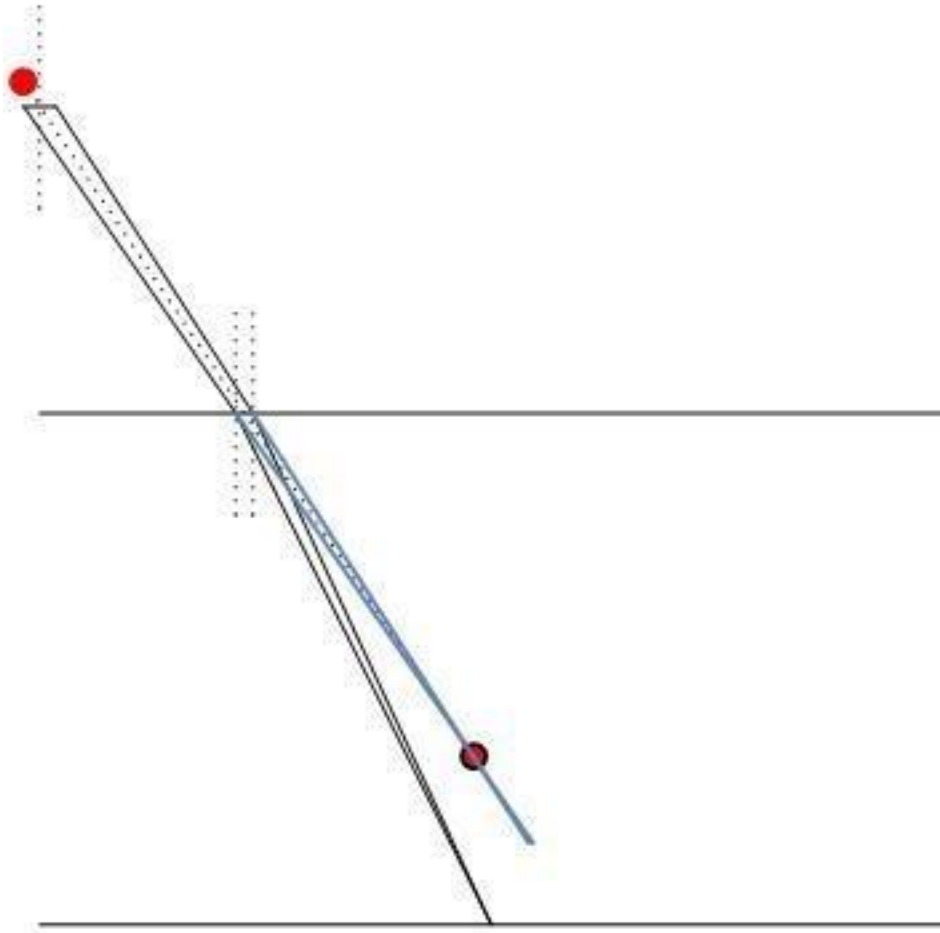


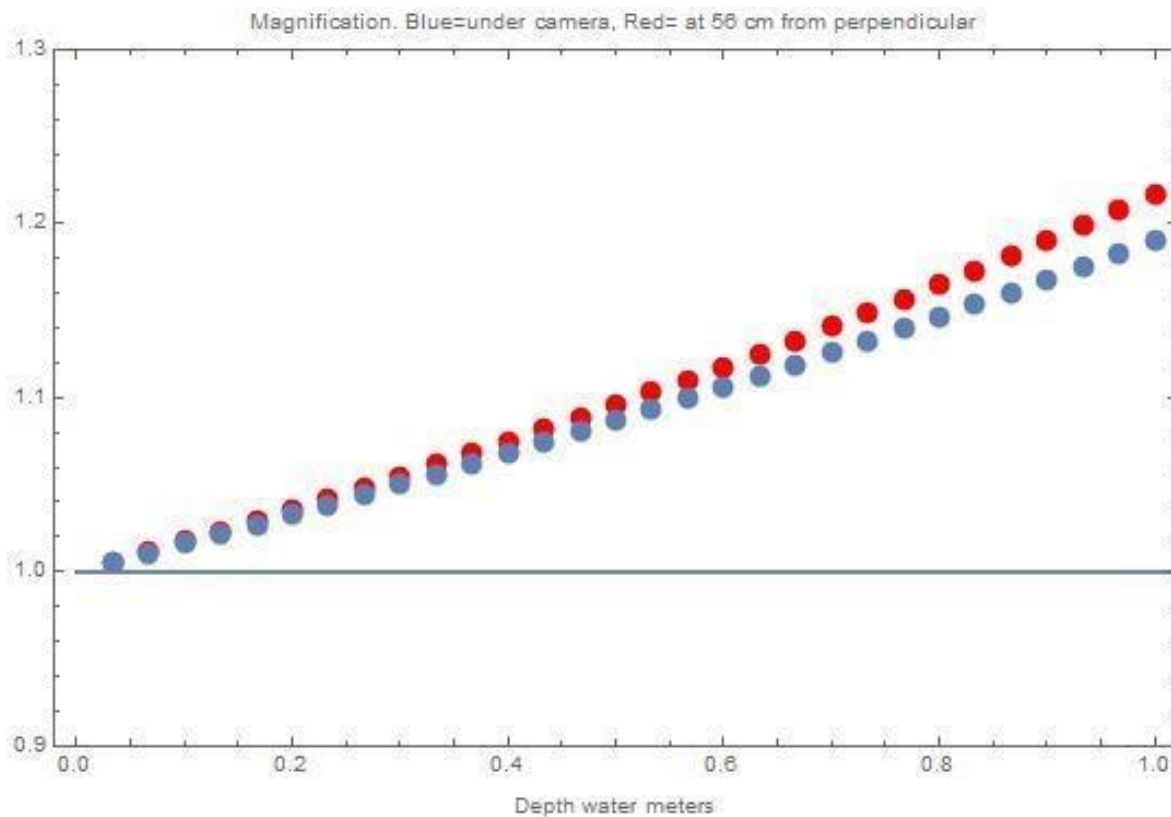
Fig. 3 Here the parameters are the same with Fig. 2 except the object at bottom is way far from the perpendicular foot, that is at  $x=56\text{cm}$ . This image is at a different scale than Fig. 2 (see for example how small is here the lens  $4\text{cm}$  diameter, even if it is the same lens as in Fig. 2)

In order to calibrate theoretically the magnification we studied the function final  $m(x)$  magnification between object on bottom and image on sensor, given by:

$$m = \frac{I(x; h, H, L, f, n)}{I(x; h, H, L, f, 1)}$$

defined as the ratio between the length of the image on sensor in the experiment, over the length of the image on sensor if there would be no water, at the same  $x$ ,  $L$ ,  $H+h$  distance, and  $f$ . That is we put object at  $x$ , fill water to  $h$ , put lens at  $H$  from water, that is  $H+h$  from bottom and measure image  $I(x; h, H, L, f, n)$ . Then we keep camera and object the same places and empty water, to do this we just make  $n=1$ . That is  $I(x; h, H, L, f, 1)$ . The ratio of these 2 is how much does the water change the image of an object placed at  $x$  at the bottom.

Below is the dependence of this ratio with the water depth,  $h$  that is  $m(h)$  for  $n=1.33$ ,  $L=4\text{cm}$ ,  $H+h=1.6\text{m}$  constant (lens has constant position from bottom) and for two  $x$  position: Blue circles  $x=6\text{cm}$ , and red circles  $x=56\text{cm}$ .



This graphics shows that we need to apply the  $x$ -correction (placement of object away from foot of perpendicular, the so called “Demirkiran correction”).